

**$B \rightarrow K^*$  form factors from flavor data to QCD and back**

Christian Hambrock,<sup>\*</sup> Gudrun Hiller,<sup>†</sup> and Stefan Schacht<sup>‡</sup>  
*Institut für Physik, Technische Universität Dortmund, D-44221 Dortmund, Germany*

Roman Zwicky<sup>§</sup>

*School of Physics and Astronomy, University of Edinburgh,  
 Edinburgh EH9 3JZ, Scotland, United Kingdom*

(Received 26 August 2013; published 4 April 2014)

Sufficient control of transition form factors is a vital ingredient for the precision flavor programs including the nearer term searches at the Large Hadron Collider and the forthcoming Belle II experiment. We improve on existing methods to extract  $B \rightarrow K^*$  form factor ratios at low hadronic recoil from  $B \rightarrow K^* \ell^+ \ell^-$  data on the angular observables  $F_L$ ,  $A_T^{(2)}$  and  $P_4'$  by adding heavy quark symmetry-based constraints and by investigating the cross talk between low and large recoil. The data-extracted form factor ratios (i) provide benchmarks for the lattice and light-cone sum rule predictions, the latter of which have been updated including improved uncertainty estimations, and (ii) allow us to improve the predictions for benchmark observables. We find that present data on the forward-backward asymmetry  $A_{FB}$  and the angular observable  $P_5'$  at low recoil are in good agreement with the Standard Model.

DOI: 10.1103/PhysRevD.89.074014

PACS numbers: 13.20.He, 12.39.Hg

**I. INTRODUCTION**

Semileptonic exclusive rare  $B$  decays are important probes of the flavor sector in and beyond the Standard Model (SM). With available event rates exceeding several hundreds first results of statistics-intense angular analyses in  $B \rightarrow K^* \mu^+ \mu^-$  decays have recently become available [1–6], allowing for a first thorough look into the physics of the  $|\Delta B| = |\Delta S| = 1$  transitions. (The  $B$ -factory sample by BABAR [1] contains electron final states as well.)

Notorious limitations of the (new) physics sensitivity stem from hadronic matrix elements, most importantly transition form factors, and their uncertainties. For  $B \rightarrow K^*$  transitions form factor estimations exist from relativistic quark models [7,8], light-cone sum rules (LCSR) [9–11] or lattice QCD [13–15]. To further validate and shape such methods, which, at the same time provide inputs to SM tests, independent information on the form factors is desirable.

As discussed in a series of papers dedicated angular observables enable one to control the form factor uncertainties [16–24] and to measure this SM background irrespective of new physics (NP) [25]. While proposals exist for the kinematic region of large hadronic recoil, at low recoil the operator product expansion (OPE) in  $1/Q$ ,  $Q = \{m_b, \sqrt{q^2}\}$  [26], recently [27], together with improved Isgur-Wise form factor relations [28] is instrumental. ( $m_b$  denotes the mass of the  $b$  quark while  $q^2$  the invariant mass-squared of the dileptons.) The low recoil

region features the additional advantage of a strong parametric suppression of the subleading  $1/m_b$  corrections to the decay amplitudes at the level of a few percent. The high predictivity of the low recoil OPE to  $\mathcal{O}(1/m_b)$  implies that its performance can be quantified experimentally. Requisite observables have been discussed recently in Ref. [29].

In a previous work two of us demonstrated the extraction of  $B \rightarrow K^*$  form factor ratios from data in the low recoil region [30], for which the outcome is in agreement with a general Bayesian fit [31]. Within this first analysis good agreement between the data-extracted ratios and the lattice estimations at low recoil as well as the LCSR results at large recoil has been obtained. Given the importance of further form factor information in view of the high statistics searches in the near term future at LHCb [32] and the forthcoming Belle II [33] experiments in this work we improve the method in several ways as follows:

- (i) Use the recent experimental  $B \rightarrow K^* \ell^+ \ell^-$  data.
- (ii) Add symmetry-based form factor relations at large recoil to the fit and detail the higher order symmetry-breaking corrections.
- (iii) Provide LCSR form factor ratios obtained by taking into account error correlations.

The plan of the paper is as follows: In Sec. II we review the relevant low recoil observables in  $B \rightarrow K^* \ell^+ \ell^-$  decays. In Secs. III A and III B we scrutinize  $B \rightarrow K^*$  form factor relations following from the equations of motion (e.o.m.) and the heavy quark expansion, respectively, which are beneficial to the LCSR predictions for form factor ratios presented in Sec. III C. Fits to data and resulting predictions for rare decay observables are presented in Secs. IV and V, respectively. We conclude in Sec. VI. Details on the  $B \rightarrow K^* \ell^+ \ell^-$  angular distribution is deferred to Appendix A. In

<sup>\*</sup> christian.hambrock@tu-dortmund.de

<sup>†</sup> gudrun.hiller@tu-dortmund.de

<sup>‡</sup> stefan.schacht@tu-dortmund.de

<sup>§</sup> Roman.Zwicky@ed.ac.uk

Appendix B we give auxiliary information on  $B \rightarrow K^*$  and  $B \rightarrow K$  form factors. In Appendix C the origin of form factor suppressions from LCSR at tree level is illustrated.

## II. $B \rightarrow K^* \ell^+ \ell^-$ OBSERVABLES AT LOW RECOIL

We briefly recapitulate in Sec. II A the benefits of certain  $B \rightarrow K^* \ell^+ \ell^-$  observables in terms of short-distance independence at low hadronic recoil. In Sec. II B we comment on the impact of right-handed flavor-changing neutral currents (FCNCs) and how this potential NP background to the form factor extractions can be controlled experimentally even further.

### A. Short-distance independence

The low recoil region is the kinematic region where the emitted  $K^*$  is soft in the  $B$ -rest frame; see Fig. 1 for a schematic of the regions of interest in  $B \rightarrow K^* \ell^+ \ell^-$  decays. The low recoil OPE [26,27] predicts at leading order a universal factorized form of the transversity amplitudes  $A_{\perp,||,0}^{L,R}$  in  $B \rightarrow K^* \ell^+ \ell^-$  decays [25],

$$A_i^{L,R}(q^2) \propto C^{L,R}(q^2) \cdot f_i(q^2) + \mathcal{O}(\alpha_s/m_b, [C_7/C_9]/m_b),$$

$$i = \perp, ||, 0. \quad (1)$$

Here, the  $C^{L,R}$  denote short-distance coefficients, which are independent of the  $K^*$  polarization. The latter is labeled by  $i = \perp, ||, 0$  denoting perpendicular, parallel and longitudinal polarization, respectively, and the superscripts  $L, R$  denote the lepton pair chirality. The form factors  $f_i$ , on the other hand, are independent of the short-distance coefficients of the  $|\Delta B| = |\Delta S| = 1$  electroweak theory.

The simple structure shown in Eq. (1) is the source of a multitude of phenomenological opportunities. Let us discuss corrections to it. As indicated in Eq. (1) the universality holds up to parametrically suppressed  $1/m_b$  corrections which originate from  $\alpha_s$  corrections to the matrix element and from the higher order Isgur-Wise

relations. The latter enter with suppression by the ratio of Wilson coefficients as  $|C_7/C_9| \lesssim 0.1$  by virtue of recent rare decay data; see, e.g., [25]. While the next-to-leading order  $1/m_b$  corrections are computed in [26], only little is known presently on the additional heavy quark form factors they depend on. Further breakings could arise from violations of quark hadron duality. Toy model estimates, however, indicate that they are negligible within current uncertainties [27]; in any case breakings of universality could be probed for experimentally [29]. For further discussion including  $c\bar{c}$ -resonance contributions, see, recently [34]. The impact of right-handed currents, which would invalidate Eq. (1), is discussed in Sec. II B.

The form factors  $f_i$ , at leading order  $1/m_b$ , are given by

$$f_{\perp} = \mathcal{N} \frac{\sqrt{2\hat{s}\hat{\lambda}}}{1 + \hat{m}_{K^*}} V, \quad f_{||} = \mathcal{N} \sqrt{2\hat{s}}(1 + \hat{m}_{K^*})A_1,$$

$$f_0 = \mathcal{N} \frac{(1 - \hat{s} - \hat{m}_{K^*}^2)(1 + \hat{m}_{K^*})^2 A_1 - \hat{\lambda} A_2}{2\hat{m}_{K^*}(1 + \hat{m}_{K^*})}. \quad (2)$$

Above we have suppressed the explicit  $q^2$  dependence of the form factors as we shall occasionally do in the rest of the paper. The hatted quantities denote:  $\hat{s} \equiv q^2/m_B^2$  and  $\hat{m}_{K^*} \equiv m_{K^*}/m_B$ , where  $m_{K^*}$  and  $m_B$  are the respective meson masses. The common normalization factor is given as [30]

$$\mathcal{N} = \mathcal{N}(\hat{s}) = G_F \alpha_e V_{tb} V_{ts}^* \sqrt{\frac{m_B^3 \sqrt{\hat{\lambda}}}{3 \times 2^{10} \pi^5}}, \quad (3)$$

where  $G_F$  denotes the Fermi constant,  $V_{ij}$  are the Cabibbo-Kobayashi-Maskawa matrix elements, and the Källén function  $\hat{\lambda} = \lambda(1, \hat{m}_{K^*}^2, \hat{s})$  reads as usual  $\hat{\lambda} = 1 + \hat{s}^2 + \hat{m}_{K^*}^4 - 2(\hat{s} + \hat{s}\hat{m}_{K^*}^2 + \hat{m}_{K^*}^2)$ . The standard form factors  $V, A_{1,2}$  are defined as

$$\langle K^*(p, \eta) | \bar{s} \gamma_{\mu} (1 - \gamma_5) b | \bar{B}(p_B) \rangle = \epsilon_{\mu\nu\rho\sigma} \eta^{*\nu} q^{\rho} p^{\sigma} \frac{2V(q^2)}{m_B + m_{K^*}} - i \eta_{\mu}^* (m_B + m_{K^*}) A_1(q^2) + i(p_B + p)_{\mu} \frac{(\eta^* \cdot q) A_2(q^2)}{m_B + m_{K^*}} + q_{\mu} \dots, \quad (4)$$

where  $\eta$  denotes the  $K^*$  polarization,  $p, p_B$  the 4-momenta of the  $K^*, \bar{B}$  mesons, respectively, and  $q = p_B - p$ .

From Eq. (1) one can obtain short-distance independent observables of the type  $(A_i^L A_j^{L*} \pm A_i^R A_j^{R*}) / (A_i^L A_k^{L*} \pm A_i^R A_k^{R*})$ ,

where  $i, j, k, l = \perp, ||, 0$ . Examples include the fraction of longitudinally polarized  $K^*$  mesons  $F_L$ , the transverse asymmetry  $A_T^{(2)}$  [16] and the angular observable  $P_4'$  [24,35], defined as

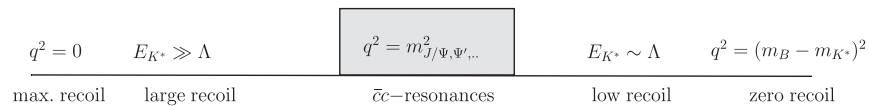


FIG. 1. The regions of interest in the physical spectrum,  $4m_{\ell}^2 \leq q^2 \leq (m_B - m_{K^*})^2$ , for  $B \rightarrow K^* \ell^+ \ell^-$  decays. The energy of the  $K^*$  meson in the  $B$  rest frame is given by  $E_{K^*} = (m_B^2 + m_{K^*}^2 - q^2)/(2m_B)$ .  $m_{\ell}$  denotes the mass of the leptons. Here we use  $\Lambda = \Lambda_{\text{QCD}}$  for the QCD scale. At low recoil the OPE captures the effect of the higher  $c\bar{c}$  resonances after sufficiently large  $q^2$  binning.

$$F_L(q^2) \equiv \frac{|A_0^L|^2 + |A_0^R|^2}{\sum_{X=L,R} (|A_0^X|^2 + |A_\perp^X|^2 + |A_\parallel^X|^2)}, \quad (5)$$

$$A_T^{(2)}(q^2) \equiv \frac{|A_\perp^L|^2 + |A_\perp^R|^2 - |A_\parallel^L|^2 - |A_\parallel^R|^2}{|A_\perp^L|^2 + |A_\perp^R|^2 + |A_\parallel^L|^2 + |A_\parallel^R|^2}, \quad (6)$$

$$P_4'(q^2) \equiv \frac{\sqrt{2} \text{Re}(A_0^L A_\parallel^{L*} + A_0^R A_\parallel^{R*})}{\sqrt{(|A_\perp^L|^2 + |A_\perp^R|^2 + |A_\parallel^L|^2 + |A_\parallel^R|^2)(|A_0^L|^2 + |A_0^R|^2)}}, \quad (7)$$

which can be measured from an angular analysis. The aforementioned low recoil OPE predicts, for fixed  $q^2$  [25],

$$\begin{aligned} F_L(q^2) &= \frac{f_0^2(q^2)}{f_0^2(q^2) + f_\perp^2(q^2) + f_\parallel^2(q^2)}, \\ A_T^{(2)}(q^2) &= \frac{f_\perp^2(q^2) - f_\parallel^2(q^2)}{f_\perp^2(q^2) + f_\parallel^2(q^2)}, \\ P_4'(q^2) &= \frac{\sqrt{2} f_\parallel(q^2)}{\sqrt{f_\parallel^2(q^2) + f_\perp^2(q^2)}}, \end{aligned} \quad (8)$$

up to the corrections indicated in Eq. (1). The ranges are  $0 \leq F_L \leq 1$ ,  $-1 \leq A_T^{(2)} \leq 1$  and  $0 \leq P_4' \leq \sqrt{2}$ . If these observables are extracted from a binned analysis, as required by the OPE and done in the subsequent fits, one inherits a residual short-distance dependence. From the angular coefficients  $J_k$ , with binned value

$$\langle J_k \rangle_{\text{bin}} \equiv \int_{\text{bin}} d^2 q^2 J_k(q^2), \quad (9)$$

one obtains for an observable  $X(J_k)$  its binned value as  $\langle X \rangle = X(\langle J_k \rangle)$ . Observables used in this work expressed in terms of the  $J_k$  and expressions for the latter can be seen in Appendix A. In the case of  $F_L$  and  $A_T^{(2)}$  the binning corresponds to simply replacing  $f_i^2(q^2)$  with  $\int_{\text{bin}} d^2 q^2 (|C^L(q^2)|^2 + |C^R(q^2)|^2) f_i^2(q^2)$ .

The short-distance coefficients drop out of Eqs. (8) in the limit of vanishing bin size only. However, since the bin-averaged change of the  $q^2$  slope due to NP does not exceed the percent level [30], the numerical impact of the binning-induced short-distance dependence is negligible given the present accuracy of the data. In the following we use the most recent data on  $F_L$ ,  $A_T^{(2)}$  and  $P_4'$  to obtain information on form factor ratios  $f_i/f_j$  by application of the binned version of Eqs. (8). Further, presently not measured low recoil observables sharing a similar short-distance insensitivity are given in [25,29]. Note that, at the point of zero recoil, where the dilepton mass is maximal,  $q_{\text{max}}^2 = (m_B - m_{K^*})^2$  and  $\hat{\lambda} = 0$ , hold

$$F_L(q_{\text{max}}^2) = \frac{1}{3}, \quad A_T^{(2)}(q_{\text{max}}^2) = -1, \quad P_4'(q_{\text{max}}^2) = \sqrt{2}, \quad (10)$$

by means of Eqs. (2) and (8). In fact, inspecting the general expressions in Ref. [29] the above endpoint relations hold model-independently. The origin of Eq. (10) and other exact predictions for angular observables is the absence of direction in  $B \rightarrow K^* \ell^+ \ell^-$  decays at zero recoil, which enforces relations between the transversity amplitudes in a general dimensions six effective Hamiltonian based on Lorentz invariance [34]; see [36] for the case of sequential decays.

## B. NP background

The extraction of form factor ratios independent of NP is based on the fact that up to few-percent corrections short-distance coefficients drop out of certain observables. As far as ratios involving  $f_\perp$  are concerned, it hinges on the assumption that no significant right-handed NP component is present. While at present there is no experimental evidence for  $V + A$  FCNCs, it is important to search for or bound such effects. Current data imply a model-independent background not exceeding  $\sim 30\%$  in  $f_\perp/f_\parallel$  [29]. If NP resides in dipole operators only, the background is reduced to  $\lesssim 15\%$ , because the dipole coefficients are generically an order of magnitude smaller than the 4-Fermi ones, and because the factor  $\sim m_b m_B / q^2$  with which the dipole operators enter the decay amplitudes gives no enhancement at low recoil, where  $q^2 \sim \mathcal{O}(m_b^2)$ . For ratios  $f_0/f_\parallel$  the method remains valid even with right-handed currents [29].

## III. $B \rightarrow K^*$ FORM FACTORS

In Sec. III A we review the origin of form factor relations from the exact QCD e.o.m. Predictions for ratios of form factors at low and maximum recoil including order  $1/m_b$  terms are given in Sec. III B. In Sec. III C we present LCSR predictions for form factor ratios at  $q^2 = 0$  by taking into account error correlations.

### A. QCD equation of motions and helicity form factors

The following two equations:

$$\begin{aligned} i\partial^\nu (\bar{s} i \sigma_{\mu\nu} b) &= -(m_s + m_b) \bar{s} \gamma_\mu b + i\partial_\mu (\bar{s} b) \\ &\quad - 2\bar{s} i \tilde{D}_\mu b, \\ i\partial^\nu (\bar{s} i \sigma_{\mu\nu} \gamma_5 b) &= -(m_s - m_b) \bar{s} \gamma_\mu \gamma_5 b + i\partial_\mu (\bar{s} \gamma_5 b) \\ &\quad - 2\bar{s} i \tilde{D}_\mu \gamma_5 b, \end{aligned} \quad (11)$$

are straightforward applications of the QCD e.o.m. of the quarks. The second equation follows from the first one by replacing  $b \rightarrow \gamma_5 b$  and  $m_b \rightarrow -m_b$  which leaves the QCD Lagrangian invariant. Equations (11) indicate that there are

relations between (axial-)vector and tensor form factors. Equations (11) can be used to compute  $1/m_b$  corrections to Isgur-Wise relations (IWR) [37] in terms of local matrix elements. The latter are known as improved Isgur-Wise relations [28].

In order to retain the simplicity of Eqs. (11) we use the same Lorentz decomposition for the derivative term as for the tensor and vector form factors as in Eq. (B1):

$$\begin{aligned} \langle K^*(p, \eta) | \bar{s}(2i\vec{D})^\mu (a + \gamma_5) b | \bar{B}(p_B) \rangle \\ = a P_1^\mu \mathcal{D}_1(q^2) + P_2^\mu \mathcal{D}_2(q^2) + P_3^\mu \mathcal{D}_3(q^2) + P_P^\mu \mathcal{D}_P(q^2). \end{aligned} \quad (12)$$

Above  $a$  denotes an arbitrary constant separating vector and axial-vector current contributions and  $P_{1,2,3,P}^\mu$  are defined in Eq. (B3). Using the decompositions Eqs. (B1) and (11) as well as the e.o.m. gives rise to four equations:

$$\begin{aligned} T_1(q^2) &= -(m_b + m_s) \mathcal{V}_1(q^2) - \mathcal{D}_1(q^2), \\ T_2(q^2) &= -(m_b - m_s) \mathcal{V}_2(q^2) - \mathcal{D}_2(q^2), \\ T_3(q^2) &= -(m_b - m_s) \mathcal{V}_3(q^2) - \mathcal{D}_3(q^2), \\ 0 &= \left( \frac{q^2}{m_b + m_s} - (m_b - m_s) \right) \mathcal{V}_P(q^2) - \mathcal{D}_P(q^2). \end{aligned} \quad (13)$$

In terms of the standard form factors  $V$ ,  $A_{0,1,2,3}$  these equations<sup>1</sup> read

$$\begin{aligned} T_1(q^2) &= c_1 V(q^2) - \mathcal{D}_1(q^2), \\ T_2(q^2) &= c_2 A_1(q^2) - \mathcal{D}_2(q^2), \\ T_3(q^2) &= \frac{c_3}{q^2} A_3(q^2) - \mathcal{D}_3(q^2), \\ 0 &= \left( c_P - \frac{c_3}{q^2} \right) A_0(q^2) - \mathcal{D}_P(q^2), \end{aligned} \quad (14)$$

with

$$\begin{aligned} c_{1(2)} &\equiv \frac{m_b \pm m_s}{m_B \pm m_{K^*}}, \\ c_3 &\equiv 2m_{K^*}(m_s - m_b), \\ c_P &\equiv \frac{-2m_{K^*}}{m_b + m_s}; \end{aligned} \quad (16)$$

see Eq. (B2) for conversion from  $\mathcal{V}_{P,1,2,3}$ . The appearance of the pole at  $q^2 = 0$  is an artifact of the decomposition.

<sup>1</sup>Equations (13) correspond to the four equations given in the Appendix of Ref. [26] in a convention of form factors adapted to low recoil, as used by Isgur and Wise [37]. The conversion between the two Lorentz decompositions for the vector/tensor and vector-derivative form factors (12) can be found in the Appendix of Ref. [26] and in Appendix B of this work, respectively.

The pole would correspond to a massless hadron with  $\bar{b}s$  flavor which is not present in the QCD spectrum. The condition  $A_0(0) = A_3(0)$  ensures that  $V$ - $A$  matrix elements (B1) are free of this pole. Since there is no structure  $P_P^\mu$  in the tensor matrix elements it follows that the  $\mathcal{D}_{P,3}$  have to cancel the pole in Eqs. (15) as illustrated in Appendix B 3. Alternatively one might add the two equations in (15):

$$\begin{aligned} T_3(q^2) &= \left[ \frac{c_3}{q^2} (A_3(q^2) - A_0(q^2)) + c_P A_0(q^2) \right] \\ &\quad - [\mathcal{D}_P(q^2) + \mathcal{D}_3(q^2)], \end{aligned} \quad (17)$$

where both terms in square brackets are regular as  $q^2 \rightarrow 0$ , which follows from  $A_0(0) = A_3(0)$  and the fact that  $T_3(q^2)$  has no  $1/q^2$  term. In fact for  $q^2 \rightarrow 0$  the equation above becomes

$$\begin{aligned} T_3(0) &= [c_3(A_3'(0) - A_0'(0)) + c_P A_0(0)] \\ &\quad - [\mathcal{D}_P(0) + \mathcal{D}_3(0)], \end{aligned} \quad (18)$$

where the prime denotes the derivative with respect to  $q^2$ .

For the subsequent discussion we introduce the helicity form factors  $f_\pm = (f_\perp \mp f_\parallel)/\sqrt{2}$  and define

$$\mathcal{D}_+(q^2) \equiv \frac{1}{\sqrt{2}} (\mathcal{D}_1(q^2) - \mathcal{D}_2(q^2)), \quad (19)$$

where the “+” subscript indicates the  $K^*$  helicity in the case where  $V$ - $A$  structure is assumed. Using the equality of  $T_1$  and  $T_2$  at  $q^2 = 0$  [Eq. (B1)] from Eqs. (2) and (14) one can show that

$$\sqrt{2} \mathcal{D}_+(0) = c_1 V(0) - c_2 A_1(0) \quad (20)$$

and

$$f_+(0) \propto \mathcal{D}_+(0) + \mathcal{O}(m_s/m_b). \quad (21)$$

## B. Helicity suppression of form factors

At large recoil empirical facts and theoretical investigations indicate that there are relations between helicity directions. As we will show, on the level of form factors this amounts to the statement (to be made more precise)

$$\mathcal{D}_+(0) = \mathcal{O}\left(\frac{\Lambda^{5/2}}{m_b^{5/2}}\right), \quad (22)$$

implying a suppression with respect to the standard form factors  $T_{1,2}(0)$  and  $V$ ,  $A_{1,2}(0)$  by one power of the heavy quark mass. At low recoil the form factors  $\mathcal{D}_{1,2}$  are separately power suppressed by virtue of the IWR. We discuss these aspects, partly, through the double ratio  $\mathcal{R}$  and its reduced part  $\hat{\mathcal{R}}$ :

$$\mathcal{R}(q^2) \equiv \frac{V(q^2)/A_1(q^2)}{T_1(q^2)/T_2(q^2)} \equiv \frac{c_2}{c_1} \hat{\mathcal{R}}(q^2), \quad (23)$$

where by means of Eq. (14)

$$\hat{\mathcal{R}}(q^2) = \frac{1 + \mathcal{D}_1(q^2)/T_1(q^2)}{1 + \mathcal{D}_2(q^2)/T_2(q^2)}. \quad (24)$$

For the subsequent discussion we write  $\hat{\mathcal{R}}$  in terms of an  $\alpha_s$  and  $1/m_b$  double expansion:

$$\begin{aligned} \hat{\mathcal{R}} &= [\hat{\mathcal{R}}_1 + \hat{\mathcal{R}}_{\alpha_s} + \dots] + [\hat{\mathcal{R}}_{1/m_b} + \hat{\mathcal{R}}_{\alpha_s/m_b} + \dots] \\ &\quad + [\hat{\mathcal{R}}_{1/m_b^2} + \dots]. \end{aligned} \quad (25)$$

We elaborate on  $\hat{\mathcal{R}}_1 = 1$  and  $\hat{\mathcal{R}}_{\alpha_s} = 0$  at large and low recoil in Secs. III B 1 and III B 2, respectively, and summarize them in Sec. III B 3.

### 1. Maximum recoil

At  $q^2 = 0$  the ratio  $\hat{\mathcal{R}}$  can be written as

$$\begin{aligned} \hat{\mathcal{R}}(0) &= 1 + \frac{\mathcal{D}_+(0)}{T} + \mathcal{O}(\Lambda^2/m_b^2), \\ \frac{\mathcal{D}_+(0)}{T} &= \mathcal{O}(\Lambda/m_b), \end{aligned} \quad (26)$$

where we have defined  $\sqrt{2}T \equiv T_{1,2}(0)$ . In the following we summarize the statements on  $\mathcal{D}_+(0)/T = \mathcal{O}(1/m_b)$ , or equivalently  $\hat{\mathcal{R}}(0) - 1 = \mathcal{O}(1/m_b)$  in the literature in chronological order and then elaborate it within LCSR.

The IWR predict that at low recoil  $\mathcal{D}_1$  and  $\mathcal{D}_2$  are both power suppressed [26,38]. The applicability of the IWR to large recoil is not straightforward as the heavy quark ceases to be static. Burdman and Donoghue [39] follow up on this question pointing out that soft contributions are not to change the relations and suggested that hard  $\alpha_s$  corrections are not to change them either. In the seminal work on the large energy limit (LEL) Charles *et al.* [40] perform a tree-level analysis and obtain symmetry relations which are even stronger than the IWR. In addition they show through explicit computation that LCSR satisfy the LEL relations at tree level. The question of whether these relations receive hard  $\alpha_s$  corrections was undertaken by Beneke and Feldmann [41] within the framework of QCD factorization (QCDF), for an investigation using soft collinear effective theory; cf., [42]. It was found that  $\mathcal{D}_+(0)$  but not  $\mathcal{D}_{1,2}(0)$  are power suppressed at order  $\alpha_s$ . An interesting observation is that endpoint sensitive contributions, which prevent a computation of the form factors *per se* in QCDF, are absent in the symmetry-breaking corrections [41], i.e., the  $\mathcal{D}_i$ . In Ref. [43] it was conjectured that to leading order in  $1/m_b$  helicity is preserved, causing a suppression of the “wrong”  $B \rightarrow K^*$  helicity amplitude  $f_+$ , and that therefore a subset of the LEL relations, which are valid for  $E_{K^*}, m_b \gg \Lambda$  [40],

$$\frac{V(q^2)}{A_1(q^2)} = \frac{(m_B + m_{K^*})^2}{2m_B E_{K^*}}, \quad \frac{T_1(q^2)}{T_2(q^2)} = \frac{m_B}{2E_{K^*}}, \quad (\text{LEL}) \quad (27)$$

does not receive corrections at any order in  $\alpha_s$ , which is consistent with an explicit  $\alpha_s^2$  computation in QCDF [44]. A consequence of the conjecture is that  $\mathcal{D}_+(0)$  is power suppressed to all orders in  $\alpha_s$ . For works exploiting the suppression of  $f_+$ , see [16,18,45–48].

Here we discuss the suppression of  $\mathcal{D}_+(0)$  within LCSR. In Ref. [49] it was shown that for the twist-2 distribution amplitude (DA)  $\phi^\perp$  [ $(\perp)$  superscript in the equation below] the relation

$$X_1^{(\perp)}(q^2) = X_3^{(\perp)}(q^2) = (1 - q^2/m_b^2)X_2^{(\perp)}(q^2), \quad (28)$$

is valid in LCSR to all order in  $\alpha_s$  for massless QCD (at the exception of the one  $b$  quark). Here the functions  $X_i(q^2)$ ,  $i = 1, 2, 3$ , are form factors of arbitrary local operators in the Lorentz decomposition of Eqs. (B1) and (12). Specifically,  $X_i$  stands for  $T_i$ ,  $\mathcal{V}_i$  or  $\mathcal{D}_i$ . Equation (28) is based on a general ansatz that is convoluted with the  $\phi^\perp$  projector and boundedness of the  $B \rightarrow K^* \ell^+ \ell^-$  decay rate for  $m_{K^*} \rightarrow 0$ ; see [50] for details. Second, the other twist-2 DA  $\phi^\parallel$  does not contribute to the  $\pm$ -helicity polarization.<sup>2,3</sup> Therefore to leading twist-2 and to all orders in  $\alpha_s$ , Eq. (28) returns  $\mathcal{D}_+^{(\perp)}(0) = 0$  and establishes the twist-2 suppression of  $\mathcal{D}_+(0)$  in LCSR. We have verified explicitly that this is true up to order  $\alpha_s$  by using the results given in [51].

We expand this discussion as it is known that the twist and heavy quark power counting do not correspond to each other. On the level of the correlation function the light-cone dominance and thus the higher twist suppression is controlled parametrically by the  $b$ -quark mass  $m_b$ . When the sum rule is constructed and the continuum threshold is introduced, higher twist contributions are suppressed by the Borel parameter. The latter is an external parameter which can be chosen at a compromise value to suppress higher twist contributions and continuum states, parameterized by the continuum threshold  $s_0$ , such that the form factor extraction is not affected significantly. At this point the role of  $m_b$  is changed from being a parametric to a numerical quantity. The twist counting does not correspond to the  $m_b$  counting anymore. This is reflected in the fact that twist-2 and twist-3 contributions do enter at the same power of the heavy quark mass when the heavy quark limit of the

<sup>2</sup>In the terminology for the DA the superscript  $\perp$  corresponds to the  $i = \perp, \parallel$  polarizations and the superscript  $\parallel$  corresponds to the  $i = 0$  helicity polarization. The reason a 0-helicity quantity appears in an  $\pm$ -helicity direction is that the DA parameters are related by the QCD e.o.m.

<sup>3</sup>The correlation functions, from which LCSR are built, satisfy the e.o.m. modulo contact terms between the operator in question and the interpolating current for the  $B$  meson. The latter are, however, independent of the four momentum squared of the  $B$  meson and therefore do not enter the dispersion relation.

type [52] is attempted. Let us remark that this is tightly connected to the Feynman mechanism, whereby the spectator quark only carries a wee momentum fraction. The latter is a nonperturbative or soft effect and related to the fact that direct perturbative approaches do not reliably capture this effect. Using the results in [51], we find though that for  $\mathcal{D}_+$  the twist-3 contributions which enter at leading order in heavy quark power counting do cancel. This might be related to the observation in [41] that endpoint divergent contributions in QCDF do not contribute to symmetry-breaking corrections. This establishes  $\hat{\mathcal{R}}_1(0) = 1$  and  $\hat{\mathcal{R}}_{\alpha_s}(0) = 0$  in LCSR. Our findings suggest that  $\mathcal{D}_+$  can be approximated by  $\mathcal{D}_+^{(0)}$  obtained using static  $b$  quarks.

Summarizing, within LCSR we have given an argument of why the leading twist-2 DA does not contribute to  $\mathcal{D}_+$  to any order in  $\alpha_s$  and we have verified up to order  $\alpha_s$  that twist-3 contributions do not contribute to leading order. Thus  $\mathcal{D}_+$  is power suppressed at least to order  $\alpha_s$  in LCSR. Let us add that the twist-2 statement also applies to QCDF, consistent with fixed order calculations [41,44]. In Appendix C the power suppression at tree level of  $\mathcal{D}_{1,2,+}(0)$  in LCSR is shown explicitly.

## 2. Low recoil

At leading order in  $1/m_b$  the two form factors  $\mathcal{D}_{1,2}$  are matched onto the static matrix elements  $\mathcal{D}_{1,2}^{(0)}$ . The e.o.m. Eqs. (14) become

$$\begin{aligned} T_1(q^2) &= \frac{(m_b \kappa_m + m_s)}{m_B + m_{K^*}} V(q^2) - \mathcal{D}_1^{(0)}(q^2) + \mathcal{O}(\alpha_s m_b^{-1/2}, m_b^{-3/2}), \\ T_2(q^2) &= \frac{(m_b \kappa_m - m_s)}{m_B - m_{K^*}} A_1(q^2) - \mathcal{D}_2^{(0)}(q^2) + \mathcal{O}(\alpha_s m_b^{-3/2}, m_b^{-5/2}), \end{aligned} \quad (29)$$

where  $\kappa_m(\mu) = 1 + \alpha_s/(4\pi)(2 \ln(\mu/m_b) + 2) + \mathcal{O}(\alpha_s^2)$  [26] incorporates the leading heavy quark matching and  $m_{B\kappa} = m_b \kappa_m$  at leading order with  $\kappa = 1 - 2\alpha_s/(3\pi) \ln(\mu/m_b)$  as in Ref. [25].

One readily obtains the scaling  $V \sim T_1 \sim m_b \mathcal{D}_1^{(0)} \sim m_b^{1/2}$  and  $A_1 \sim T_2 \sim m_b \mathcal{D}_2^{(0)} \sim m_b^{-1/2}$  [26,37]. For completeness we give as well the relations for  $A_3$  and  $A_0$  corresponding to Eq. (15):

$$\begin{aligned} T_3(q^2) &= \frac{2m_{K^*}(m_s - m_b \kappa_m)}{q^2} A_3(q^2) - \mathcal{D}_3^{(0)}(q^2) + \mathcal{O}(\alpha_s m_b^{-1/2}, m_b^{-3/2}), \\ 0 &= -2m_{K^*} \left( \frac{1}{m_s + m_b} + \frac{m_s - m_b \kappa_m}{q^2} \right) A_0(q^2) - \mathcal{D}_P^{(0)}(q^2) + \mathcal{O}(\alpha_s m_b^{-3/2}, m_b^{-5/2}). \end{aligned} \quad (30)$$

It is straightforward to arrive at

$$\begin{aligned} \hat{\mathcal{R}}(q^2)_{E_{K^*} \sim \Lambda} &= 1 + \left( \frac{\mathcal{D}_1^{(0)}(q^2)}{T_1(q^2)} - \frac{\mathcal{D}_2^{(0)}(q^2)}{T_2(q^2)} \right) \\ &+ \mathcal{O}(\alpha_s/m_b, 1/m_b^2), \end{aligned} \quad (31)$$

and therefore  $\hat{\mathcal{R}}_1 = 1$  and  $\hat{\mathcal{R}}_{\alpha_s} = 0$  at low recoil. The heavy quark scaling between  $\mathcal{D}_{1,2}^{(0)}$  and  $T_{1,2}$  is not changed at any order in  $\alpha_s$  by virtue of heavy quark effective theory power counting.

## 3. Synthesis of maximum and low recoil region

The ratio  $\hat{\mathcal{R}}$  (23) assumes the same leading order term at maximum (26) and at low recoil (31):

$$\hat{\mathcal{R}} = 1 + \mathcal{O}(\Lambda/m_b), \quad (32)$$

despite the different heavy quark scaling of the form factors at low and large recoil, as summarized in Table I. In addition we observe that the LEL relations themselves

Eq. (27) give  $\mathcal{R}(q^2)|_{\text{LEL}} = 1 + \mathcal{O}(\Lambda/m_b)$ , that is, a constant of order one. Therefore, Eq. (26) and hence (32) extends to higher  $q^2$  above maximum recoil to the extent that LEL is still a good description, before it coincides at low recoil and leading power with the IWR prediction.

We emphasize that at  $\mathcal{O}(\alpha_s^0)$  the  $\mathcal{D}_{1,2}(0)$  are power suppressed with respect to the standard form factors and thus consistent with the IWR. This has been indirectly verified by Charles *et al.* by showing that the LCSR tree-level results obey the LEL relation of which the IWR are a subset. We should add, as previously discussed, that in [41] it was found that in QCDF  $\alpha_s$  corrections contribute at leading power to  $\mathcal{D}_{1,2}(0)$ , but not to  $\mathcal{D}_+(0)$ .

## C. LCSR prediction for form factor ratios at maximum recoil

In this section we provide an update of form factor ratios, entering (2), at maximum recoil ( $q^2 = 0$ ) using the LCSR [10] which include up to twist-3 radiative corrections. The improvement over taking the ratio of the form factors from

TABLE I. Heavy quark scaling of the form factors appearing in the e.o.m. Eq. (14). The low recoil results are the well known Isgur-Wise scaling relations for  $V$ ,  $A_1$  and  $T_{1,2}$  [37] and the ones for  $\mathcal{D}_i^{(0)}$  were stated in [26]. The large recoil results for the standard form factors are based on LCSR computations, e.g., [9,10]. The tree level and  $\mathcal{O}(\alpha_s) m_b$  scaling of  $\mathcal{D}_{1,2}$  are based on [40,41], respectively.

	$T_1(q^2)$	$V(q^2)$	$\mathcal{D}_1[\mathcal{D}_1^{(0)}](q^2)$	$T_2(q^2)$	$A_1(q^2)$	$\mathcal{D}_2[\mathcal{D}_2^{(0)}](q^2)$	$\mathcal{D}_+(q^2)$
Large recoil	$m_b^{-3/2}$	$m_b^{-3/2}$	$m_b^{-5/2} + \mathcal{O}(\alpha_s)m_b^{-3/2}$	$m_b^{-3/2}$	$m_b^{-3/2}$	$m_b^{-5/2} + \mathcal{O}(\alpha_s)m_b^{-3/2}$	$m_b^{-5/2}$
Low recoil	$m_b^{1/2}$	$m_b^{1/2}$	$m_b^{-1/2}$	$m_b^{-1/2}$	$m_b^{-1/2}$	$m_b^{-3/2}$	$m_b^{-1/2}$

[10] consists in updated hadronic parameters taken from [49], as well as the fact that ratios have correlated and therefore smaller parametric and systematic uncertainties. The latter has, for instance, been exploited in  $T_1^{B \rightarrow K^*}(0)/T_1^{B \rightarrow \rho}(0)$  [53].

The updated hadronic parameters include LCSR and lattice computation of Gegenbauer moments, quark masses from the Particle Data Group (PDG) [54] averages and a new value of  $f_{K^*}^{\parallel}$  due to updated experimental results in [54]. Summarizing the values:  $\mu_F^2 = (m_B^2 - m_b^2) \pm 1 \text{ GeV}^2$ ,  $\{f_{K^*}^{\parallel}, f_{K^*}^{\perp}\} = \{0.211(7), 0.163(8)\} \text{ MeV}$ ,  $\{a_1^{\parallel}, a_1^{\perp}, a_2^{\parallel}, a_2^{\perp}\}_{K^*} = \{0.06(4), 0.04(3), 0.16(9), 0.10(8)\}$ ,  $\{m_b, m_s\} = \{4.7(1), 0.094(3)\} \text{ GeV}$ ,  $\langle \bar{q}q \rangle = (-0.24(1) \text{ GeV})^3$  and the scale-dependent quantities, at the exception of the quark masses, are evaluated at the renormalization scale  $\mu = 1 \text{ GeV}$ .

So far we have omitted the Borel parameter  $M^2$  and the effective continuum threshold  $s_0$  in our discussion. This is where the e.o.m. in (20) bring in a new aspect. Equation (20) is exact and the same relation is going to be true at the level of the relevant correlation functions, modulo the irrelevant contact terms mentioned earlier, since the light-cone OPE is compatible with or partly built on the QCD e.o.m. Thus (20) can be satisfied trivially by setting  $M_F^2$  and the effective continuum thresholds  $s_0^F$  equal for all  $F = V, A_1, \mathcal{D}_{1,2}$ . Generally though there could be significant balancing between the terms. Yet, since  $|\mathcal{D}_+(0)| \ll |V(0)|, |A_1(0)|$  [see Eq. (26)], this implies  $\{M_V^2, s_0^V\} \approx \{M_{A_1}^2, s_0^{A_1}\}$ . Let us be slightly more precise by making the argument in two steps. First semiglobal quark hadron duality implies that the continuum thresholds of  $A_1, V, \mathcal{D}_+$  are all somewhere between, say,  $(m_B + m_{\pi} + m_K)^2$  and  $(m_B + m_{K^*})^2$ . Second if we offset  $s_0^{A_1}$  from  $s_0^V$  by a significant amount, then due to the smallness of  $\mathcal{D}_+$  this can only be balanced by an ever larger value of  $s_0^{\mathcal{D}_+}$  which would contradict step one. In view of this chain of arguments we take the average of the continuum thresholds as  $s_0^{A_1} = s_0^V = (35 \pm 1) \text{ GeV}^2$  and the Borel parameters as  $M_{A_1}^2 = M_V^2 \approx (9.0 \pm 1.5) \text{ GeV}^2$  [10]. The latter value corresponds to  $M_{\text{LC}}^2$  in [10]. The same values are taken for  $A_2$  though it can, only partly, be justified from the e.o.m. being an admixture of  $\pm$  and 0-helicity polarization. One might argue that  $s_0^{A_2} = s_0^{A_1}$  and  $M_{A_2}^2 = M_{A_1}^2$  are consistent with the fact that the intermediate states in the  $B$ -meson channel carry the same quantum numbers. In essence the somewhat weaker argument here will simply result in larger

parametric uncertainties in  $s_0^{A_2}$  and  $s_0^{A_1}$  in the corresponding form factor ratio.

We obtain the following numerical values for the form factor ratios at  $q^2 = 0$ :

$$\begin{aligned} \mathcal{R}(0) &= \frac{V(0)}{A_1(0)} = 1.31 \pm 0.10, \\ \mathcal{R}'(0) &\equiv \frac{A_2(0)}{A_1(0)} = 0.83 \pm 0.08, \end{aligned} \quad (33)$$

with 8% and 10% relative uncertainty, respectively. We have also determined  $[f_0(\hat{s})/f_{\parallel}(\hat{s})] \cdot \sqrt{\hat{s}} \xrightarrow{\hat{s} \rightarrow 0} 0.83 \pm 0.09$ , where  $s_0^{f_0}$  and  $s_0^{f_{\parallel}}$  are treated analogously to the other ratios. Each uncertainty consists of two parts, a parametric uncertainty,  $\Delta_{\text{para}}$ , and a systematic uncertainty due to quark hadron duality,  $\Delta_{s_0}$ , which have been added linearly to arrive at Eq. (33):

$$\Delta_{\mathcal{R}^{(i)}(0)} = \Delta_{\text{para}} + \Delta_{s_0}. \quad (34)$$

The parametric uncertainties correspond to all parameters except the continuum thresholds as described above. We add those uncertainties in quadrature  $\Delta_{\text{para}} = (\sum_i \Delta_i^2)^{1/2}$  as we do not see any special reasons for correlations.<sup>4</sup> Noticeable uncertainties come from  $m_b$  and the Borel mass  $M^2$ , which add up to one below the 2% level. The uncertainty due to the continuum threshold is treated in a conservative way. For the quantity  $\mathcal{R}(0)$  we vary the threshold separately,  $s_0^V = (35 \pm 1) \text{ GeV}^2$  and  $s_0^{A_1} = (35 \pm 1) \text{ GeV}^2$ , and add the uncertainties linearly as  $\Delta_{s_0} = \Delta_{s_0^V} + \Delta_{s_0^{A_1}}$ . The quantity  $\mathcal{R}'(0)$  is treated in an analogous manner.

With this treatment the bulk part, about 6(8)% out of the 8(10)% for  $\mathcal{R}(0)(\mathcal{R}'(0))$ , of the uncertainty comes from

<sup>4</sup>The exception being the errors of the parallel- and perpendicular-type Gegenbauer moments which are assumed to be fully correlated. This can be justified by inspecting the sum rules for the first Gegenbauer moments in Ref. [12]. The bulk part is due to the perturbative part and the strange quark condensate which are the same, or almost the same, respectively. Since the sum rules for the Gegenbauer moment exhibit a mild, relative, dependence on the effective continuum threshold this suggests that the errors are highly correlated. If the Gegenbauer moments are varied separately, the uncertainty in  $\mathcal{R}'(0)$ , but not in  $\mathcal{R}(0)$ , raises considerably.

$\Delta_{s_0}$ . When the continuum thresholds are varied in a correlated way, imposing  $s_0^V = s_0^{A_1}(s_0^{A_1} = s_0^{A_2})$ , then  $\Delta_{s_0}$  drops in both ratios below the 2% level. This might well be the procedure to follow as the discussion of the previous section suggests. Therefore we feel justified to say that the estimate Eq. (33) is on the conservative side by varying the thresholds separately and adding the corresponding uncertainties linearly.

Let us compare the results Eq. (33) with previous LCSR predictions from [10], where  $\{\mathcal{R}(0), \mathcal{R}'(0)\}_{[10]} \approx \{1.40, 0.88\}$ . This amounts in both ratios to a downwards shift of the central values of 7%. The reasons are the modified input parameters from theory, a new value of  $f_{K^*}^{\parallel}$  from PDG [54] as well as improved knowledge on the correlation between the effective continuum thresholds as discussed at the beginning of this section.

#### IV. FITTING FORM FACTORS

We perform fits to  $B \rightarrow K^* \ell^+ \ell^-$  data at low recoil and extract ratios of form factors. In Sec. IV A we describe the parametrization used. Details of the fit are given in Sec. IV B. Fit results are presented in Sec. IV C.

##### A. Form factor series expansion

Following Ref. [30], we parametrize the transversity form factors  $f_i$ ,  $i = \perp, 0, \parallel$ , in  $B \rightarrow K^* \ell^+ \ell^-$  decays through a series expansion (SE) [55–61]

$$f_i \propto \sum_{k=0}^{N-1} \alpha_{i,k} z^k(t), \quad (35)$$

in the variable  $z$  defined as

$$z(t) \equiv z(t, t_0) = \frac{\sqrt{t_+ - t} - \sqrt{t_+ - t_0}}{\sqrt{t_+ - t} + \sqrt{t_+ - t_0}}. \quad (36)$$

Here,  $t$  denotes the analytic continuation of  $q^2$  to the complex plane,  $t_{\pm} = (m_B \pm m_{K^*})^2$  and  $t_0$  is a free parameter in the range  $0 \leq t_0 < t_+$  for which a common choice is  $t_0 = t_{\text{opt}}$  with  $t_{\text{opt}} = t_+(1 - \sqrt{1 - t_-/t_+})$  [61,62]. Note that  $|z| \leq 1$  and  $z(t_0) = 0$ . We show  $z(t, t_0)$  in Fig. 2. How many orders of the series expansion (35) are needed for a description depends, from a pragmatic viewpoint, on the precision of the data.

To lowest order SE (SE1), the form factors are parameterized as

$$\begin{aligned} f_{\perp}(t) &= \alpha_{\perp} \Lambda(t, m_{1-}^2) \sqrt{-z(t, 0)} \sqrt{z(t, t_-)}, \\ f_{\parallel}(t) &= \alpha_{\parallel} \Lambda(t, m_{1+}^2) \sqrt{-z(t, 0)}, \\ f_0(t) &= \alpha_0 \Lambda(t, m_{1+}^2), \end{aligned} \quad (37)$$

with

$$\Lambda(t, m_R^2) = \frac{\mathcal{N}(t)}{z(t, m_R^2) \phi_T^{V-A}(t)}, \quad \alpha_i \equiv \alpha_{i,0}. \quad (38)$$

In our numerical evaluations we take  $m_{1-} = 5.42$  GeV for the vector ( $\perp$ ) and  $m_{1+} = 5.83$  GeV for the axial vector ( $\parallel, 0$ ) transitions [54].

It turns out that within SE1 several relations hold between the expansion coefficients and the full QCD form factors, and that this ansatz is actually quite constrained. Note, at this order there is no dependence on  $t_0$ . Specifically,

$$\frac{f_{\perp}(q^2)}{f_{\parallel}(q^2)} = \frac{\alpha_{\perp} z(q^2, m_{1+}^2)}{\alpha_{\parallel} z(q^2, m_{1-}^2)} \sqrt{z(q^2, t_-)} \quad (39)$$

and

$$\frac{\alpha_{\perp}}{\alpha_{\parallel}} = \frac{\sqrt{\hat{\lambda}}}{(1 + \hat{m}_{K^*})^2} \frac{z(q^2, m_{1-}^2)}{z(q^2, m_{1+}^2)} \frac{1}{\sqrt{z(q^2, t_-)}} \frac{V(q^2)}{A_1(q^2)}. \quad (40)$$

Numerically, it follows at  $q^2 = 0$

$$\frac{\alpha_{\perp}}{\alpha_{\parallel}} = 1.19 \frac{V(0)}{A_1(0)}. \quad (41)$$

This relation allows one to determine  $A_T^{(2)}$  from  $V(0)/A_1(0)$  and vice versa within SE1. Furthermore, within SE1 the constraint from  $F_L$  Eq. (10) implies (note that this has not been taken into account in [30])

$$\frac{\alpha_0}{\alpha_{\parallel}} = \sqrt{\frac{-z(t_-, 0)}{2}} = 0.29 \quad (42)$$

and

$$\begin{aligned} \frac{A_2(0)}{A_1(0)} &= \frac{1}{(1 - \hat{m}_{K^*})^2} \left( 1 - \hat{m}_{K^*}^2 - 4\sqrt{2}\hat{m}_{K^*}(1 + \hat{m}_{K^*}) \left( \frac{\alpha_0}{\alpha_{\parallel}} \right) \right) \\ &= 1.41 - 1.63 \left( \frac{\alpha_0}{\alpha_{\parallel}} \right). \end{aligned} \quad (43)$$

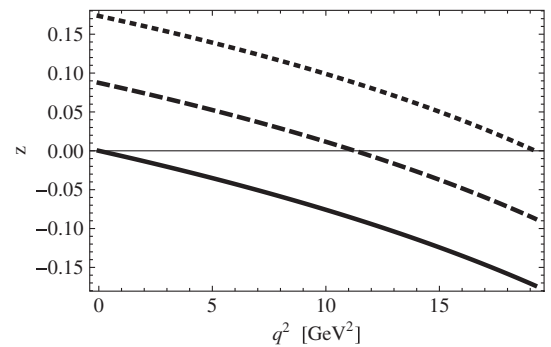


FIG. 2.  $z(t, t_0)$  as a function of  $q^2$  in  $\text{GeV}^2$  for  $t_0 = t_-, t_{\text{opt}}$  and  $t_0 = 0$ , from top to bottom, respectively.

TABLE II. High- $q^2$  data on  $B \rightarrow K^* \ell^+ \ell^-$  observables  $F_L, A_T^{(2)}$  and  $P'_4$  from BABAR [1], CDF [2], LHCb [3,6], ATLAS [4] and CMS [5] as used in this work. The statistical and systematic uncertainties are added in quadrature. The maximum  $q^2$  value in units of  $\text{GeV}^2$  equals  $X = 19$  for LHCb, ATLAS and CMS and is the endpoint otherwise.

$q^2$ [ $\text{GeV}^2$ ]	BABAR	CDF		LHCb		ATLAS	CMS	
	$F_L$	$F_L$	$A_T^{(2)}$	$F_L$	$A_T^{(2)}$	$F_L$	$F_L$	
[14,18, 16]	$0.43^{+0.13}_{-0.16}$	$0.40^{+0.12}_{-0.12}$	$0.11^{+0.65}_{-0.65}$	$0.33^{+0.08}_{-0.08}$	$0.07^{+0.26}_{-0.28}$	$-0.18^{+0.54}_{-0.70}$	$0.28^{+0.16}_{-0.16}$	$0.53^{+0.12}_{-0.12}$
[16, X]	$0.55^{+0.15}_{-0.17}$	$0.19^{+0.14}_{-0.13}$	$-0.57^{+0.60}_{-0.57}$	$0.38^{+0.09}_{-0.08}$	$-0.71^{+0.36}_{-0.26}$	$0.70^{+0.44}_{-0.52}$	$0.35^{+0.08}_{-0.08}$	$0.44^{+0.08}_{-0.08}$

<sup>a</sup>The values quoted differ from the LHCb ones by a factor  $-2$  to match the definition in Eq. (7).

Using Eq. (42) it follows  $A_2(0)/A_1(0) = 0.93$ . This is at variance with the LCSR findings Eq. (33). The reason is the simple  $q^2$  dependence of SE1. We discuss this further in Sec. IV C.

To accommodate more involved  $q^2$  shapes we go to next order in the SE (SE2). Specifically we extend Eq. (37) as

$$\begin{aligned}
 f_{\perp}(t) &= \alpha_{\perp} \Lambda(t, m_{1-}^2) \sqrt{-z(t, 0)} \sqrt{z(t, t_{-})} (1 + p_{\perp} z(t, t_0)), \\
 f_{\parallel}(t) &= \alpha_{\parallel} \Lambda(t, m_{1+}^2) \sqrt{-z(t, 0)} (1 + p_{\parallel} z(t, t_0)), \\
 f_0(t) &= \alpha_0 \Lambda(t, m_{1+}^2) (1 + p_0 z(t, t_0)),
 \end{aligned}
 \tag{44}$$

where  $p_i \equiv \alpha_{i,1}/\alpha_{i,0}$ , introducing in total three additional fit parameters  $p_i$ ,  $i = \perp, \parallel, 0$ , and dependence on  $t_0$  through  $z(t)$  in Eq. (36).

For  $t_0$  near the endpoint  $t_{-}$ ,  $z(t)$  is close to its zero crossing, and there is reduced sensitivity to the  $p_i$  in the low recoil fit. On the other hand,  $z(t)$  is more significant at large recoil; see Fig. 2. Alternatively, choosing  $t_0 \ll m_b^2$  gives high sensitivity to the low recoil fit, but has smaller impact at large recoil. We study the impact of different values of  $t_0$  numerically in Sec. IV C. Note that for  $t_0 = 0$  the relations Eqs. (41) and (43) remain valid within higher order SE if the  $\alpha_i$  are identified with the respective lowest order coefficients  $\alpha_{i,0}$ .

### B. Details of the fit

We perform a fit to the current experimental data on  $F_L, A_T^{(2)}$  and  $P'_4$ , given in Table II and include several theoretical constraints, explained in the previous sections. The observables are defined in Eq. (8), while the form factors are taken at leading order (SE1) (37) and next-to-leading order (SE2) (44). The endpoint relations (10) are included in the fits. We perform fits with LCSR input, or with LEL input, or with none. The LCSR input is given by Eq. (33). The LEL input is given by Eq. (27) evaluated at  $q^2 = 0$ :

$$\left. \frac{V(0)}{A_1(0)} \right|_{\text{LEL}} = 1.37 \pm 0.40.
 \tag{45}$$

Here we assumed an uncertainty of 30% from  $1/m_b$  corrections accounting for the absence of precise predictions for  $\mathcal{D}_+^{(0)}$ ; see Eq. (26). Furthermore, we perform a “full” fit in SE2, where in addition to the data and the LCSR

ratio Eq. (33) we include the lattice results [15] for  $V, A_1$  and  $A_2$  (the latter is given implicitly only). For the lattice data we assume an overall error correlation of 75%<sup>5</sup> and take into account 5% systematic uncertainties by adding them linearly to the statistical ones.

We perform a  $\chi^2$  fit and adopt noncorrelated Gaussian errors for the data, while the theory uncertainties in the fit are treated within the  $R$ -fit scheme [63]. The fits are performed using the LUCY code [64], which is executed with MATHEMATICA and generates C++ code in an automated way. The C++ code is linked to the NLOPT 2.3 library [65], which performs the numerical minimization. For the minimization of the  $\chi^2$  function we use the Sbplx/Subplex algorithms [65,66].

### C. Results

We show  $F_L, A_T^{(2)}, P'_4$  and the extracted values of the form factor ratios  $f_0/f_{\parallel}, f_{\perp}/f_{\parallel}, V/A_1$  and  $A_2/A_1$  in Figs. 3–9. The corresponding values of the SE parameters and resulting form factor ratios are given in Table III.

We summarize the findings of the fits:

- (i) All parameterizations describe the low recoil data for  $F_L$  and  $A_T^{(2)}$  in the low recoil region well; see Figs. 3 and 4.
- (ii) The deviations in  $P'_4$  in particular in the lower bin (see Fig. 5) go along with the observation that the  $\chi^2$  value decreases significantly in all fits by about  $\mathcal{O}(5-10)$  once  $P'_4$  is removed from the fit. The effect of  $P'_4$  in the fit is insignificant for the parameter determination.
- (iii) The results in plain SE1 are consistent with the previous findings of Ref. [30], but not equal due to the different  $B \rightarrow K^* \ell^+ \ell^-$  data. The current data gives lower values of  $V/A_1$ .
- (iv) The SE1 fit returns a value of  $V(0)/A_1(0)$  which is somewhat higher than expected from LCSR Eq. (33) and heavy quark large energy Eq. (27) predictions, although it is in agreement within uncertainties (at  $\sim 1\sigma$ ); see Table III.
- (v) Within SE1 the ratios  $A_2/A_1$  and  $f_0/f_{\parallel}$  are fixed by the parameterization for all  $q^2$ ; see also Figs. 6

<sup>5</sup>We thank Matthew Wingate for discussions on this point.

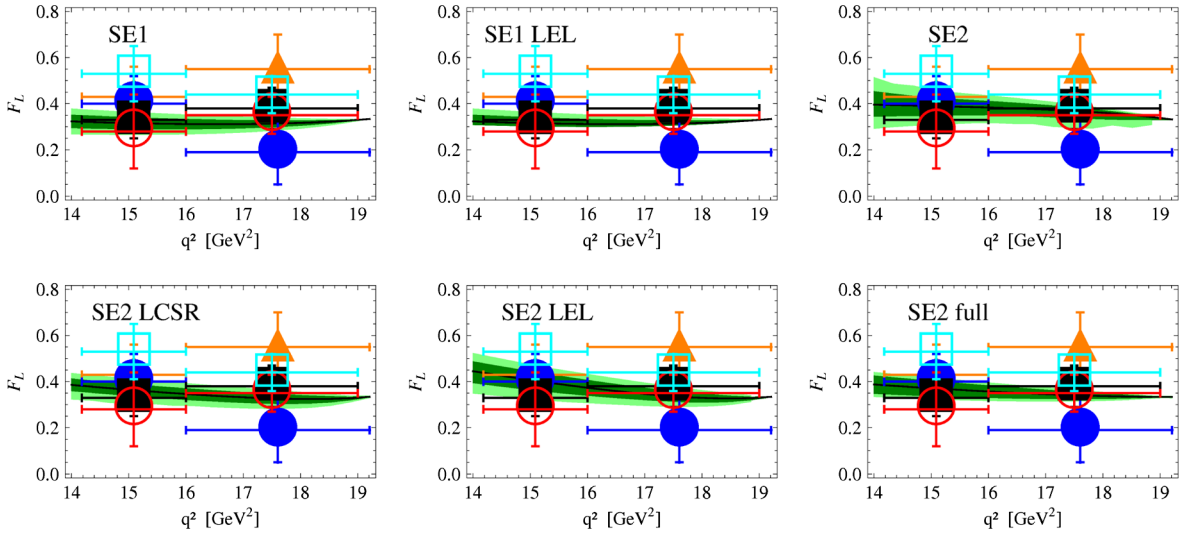


FIG. 3 (color online). Current data on  $F_L$  by *BABAR* (orange triangles), CDF (blue circles), LHCb (black squares), ATLAS (cyan hollow squares) and CMS (red hollow circles) together with the fit results. LEL and LCSR indicate that the constraints Eq. (45) and Eq. (33), respectively, have been taken into account in the  $R$ -fit scheme. “full” indicates that in addition to the data and LCSR input Eq. (33) the lattice results given in [15] have been taken into account. The SE1 LCSR fit is inconsistent, i.e., does not work and is not shown; see text for details. The (dark green) light green bands denote the (68%) 95% C.L. regions. The solid black curve corresponds to the best fit result.

and 9. Related to this is the observation that the SE1 fit with LCSR input Eq. (33) does not converge, i.e., returns a huge  $\chi^2$  because the  $R$ -fit scheme used cannot resolve the  $> 1\sigma$  tension between  $A_2(0)/A_1(0)$  in SE1 and the corresponding LCSR value.

- (vi) The issues with the simpler SE1 parametrizations mentioned in the previous item are familiar ones with the single pole ansatz of vector meson dominance (VMD). We recall that in  $B \rightarrow \pi$  studies within LCSR [51] it was found that VMD is insufficient to describe higher  $q^2$  data. In fact, even low- $q^2$  data are insufficiently described as the

residue of the  $B^*$  pole is known from lattice as well as through experiment and heavy quark scaling [51]. To sharpen this further, we repeated the fit within the simplified series expansion at lowest order (SSE1) [60], which resembles VMD. SSE1 corresponds to SE1 with the changes  $z(t, m_R^2) \rightarrow 1 - t/m_R^2$ ,  $\sqrt{-z(t, 0)} \rightarrow \sqrt{t}/m_B$  and  $\sqrt{z(t, t_-)} \rightarrow \sqrt{\hat{\lambda}}$  in Eq. (37). The following relations hold within SSE1:  $\alpha_\perp/\alpha_\parallel = 0.73[V(0)/A_1(0)]$ ,  $\alpha_0/\alpha_\parallel = 0.59$  and  $A_2(0) = A_1(0)$ . The fit (see Table III) performs worse than SE1 and exhibits larger conflicts with LCSR.

TABLE III. Results of the fits in first order (SE1) and second order (SE2) series expansion to the data given in Table II. “LEL” and “LCSR” indicate that the constraints Eq. (45) and Eq. (33), respectively, have been taken into account in the  $R$ -fit scheme. “full” indicates that in addition to the data and LCSR input Eq. (33) the lattice results given in [15] have been taken into account. In the SE2 full fit we obtain for the additional fit parameter the result  $\alpha_\parallel = -0.07^{+0.01}_{-0.02}$ . SE2 fits have been performed with  $t_0 = 0$ . The SE1 fit with LCSR input does not work and is therefore not given. The last row corresponds to a fit in SSE1 that is given for illustration only. See text for details.

Fit	$\chi^2/\text{d.o.f.}$	$\alpha_\perp/\alpha_\parallel$	$\alpha_0/\alpha_\parallel$	$p_\parallel$	$p_\perp$	$p_0$	$V(0)/A_1(0)$	$A_2(0)/A_1(0)$
SE1	20.5/14	$1.88^{+0.34}_{-0.34}$	$0.29^a$				$1.58^{+0.29}_{-0.29}$	$0.93^a$
SE1 LEL	20.5/15	$1.88^{+0.18}_{-0.34}$	$0.29^a$				$1.58^{+0.15}_{-0.29}$	$0.93^a$
SE2	12.2/11	$7.02^{+3.50}_{-4.27}$	$0.87^{+0.04}_{-0.35}$	$-1.99^{+3.79}_{-6.92}$	$3.84^{+0.00}_{-6.09}$	$3.14^{+0.37}_{-2.29}$	$5.90^{+2.99}_{-3.64}$	$0.00^{+0.57}_{-0.00}$
SE2 LCSR	15.8/13	$1.68^{+0.00}_{-0.24}$	$0.40^{+0.00}_{-0.04}$	$2.85^{+0.36}_{-2.20}$	$1.50^{+1.04}_{-3.71}$	$3.64^{+0.06}_{-1.60}$	$1.41^{+0.00}_{-0.20}$	$0.75^{+0.06}_{-0.00}$
SE2 LEL	13.6/12	$2.06^{+0.00}_{-0.95}$	$0.87^{+0.06}_{-0.41}$	$-2.89^{+5.28}_{-8.16}$	$-5.96^{+7.92}_{-24.45}$	$2.81^{+0.77}_{-2.73}$	$1.73^{+0.00}_{-0.80}$	$0.00^{+0.67}_{-0.00}$
SE2 full	21.0/(12 + 10 <sup>b</sup> )	$1.68^{+0.00}_{-0.24}$	$0.36^{+0.04}_{-0.06}$	$1.91^{+0.84}_{-1.00}$	$2.07^{+0.63}_{-0.96}$	$2.62^{+0.73}_{-1.09}$	$1.41^{+0.00}_{-0.20}$	$0.82^{+0.09}_{-0.07}$
SSE1	22.2/14	$1.16^{+0.22}_{-0.22}$	$0.59^a$				$2.28^{+0.44}_{-0.43}$	$1^a$

<sup>a</sup>Fixed within parametrization.

<sup>b</sup>Number of lattice points.

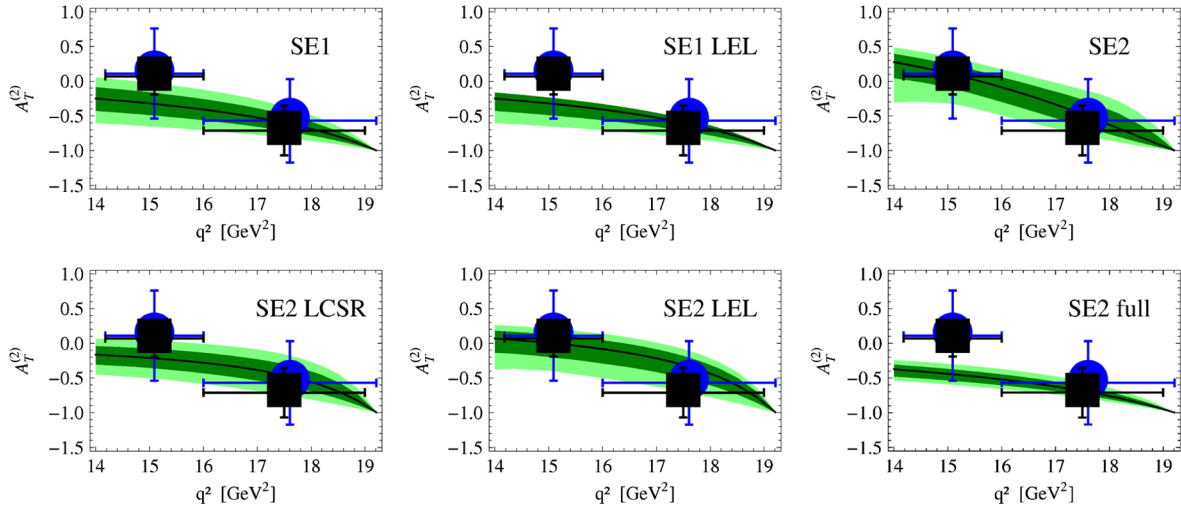


FIG. 4 (color online). Current data on  $A_T^{(2)}$  by CDF (blue circles) and LHCb (black squares) together with the fit results; see Fig. 3.

- (vii) All SE2 fits have been performed with  $t_0 = 0$ . We checked that while changing the fit parameters a different value of  $t_0$  does not change the qualitative features and the figures.
- (viii) In all SE2 fits with  $t_0 = 0$  Eqs. (41) and (43) hold, as they should.
- (ix) Within SE2 or higher some large recoil input is required to be predictive at large recoil; see Figs. 6–9. This highlights the importance of theory input for  $V(0)/A_1(0)$ .
- (x) As is well known the sensitivity to  $A_2$  is very low towards the endpoint (see Fig. 9) as  $A_2$  is multiplied by  $\sqrt{\hat{\lambda}}$  which vanishes towards the endpoint. Note that at low recoil  $A_1/A_2 = \mathcal{O}(1/m_b)$  and both terms in the numerator of  $f_0$  are  $\mathcal{O}(1/m_b^2)$  due to the kinematic factors  $E_{K^*}/m_B = \mathcal{O}(1/m_b)$  in the  $B$  rest frame, and  $f_0/f_{\parallel} = \mathcal{O}(1)$ .
- (xi) Ratios of the transversity form factors  $f_0/f_{\parallel}$  and  $f_{\perp}/f_{\parallel}$  are well behaved at low recoil always; see

Figs. 6 and 7, respectively. Note that  $f_0(q_{\max}^2)/f_{\parallel}(q_{\max}^2) = 1/\sqrt{2}$  by means of Eq. (10).

Good fits (see Table III) are obtained in the SE2, SE2 LEL and SE2 LCSR scenarios, corresponding to  $\chi^2/\text{d.o.f.}$  equal 1.11, 1.13 and 1.22, respectively. The latter two fits are advantageous with respect to the former because their predictive power extends to large recoil. As argued previously, the SE1 fits are quite constrained by their simpler parameterization and yield larger  $\chi^2/\text{d.o.f.}$  The SE2 full fit exhibits the smallest  $\chi^2/\text{d.o.f.} = 0.95$  if individual lattice points are counted separately. It relies on the data given in [15] with systematic errors of 5% added linearly to the statistical ones. The SE2 full fit serves here as a preview of the obtainable precision in the future. In view of this, we consider the three fits SE2, SE2 LEL and SE2 LCSR, with increasing input, as the best ones for further low recoil analyses.

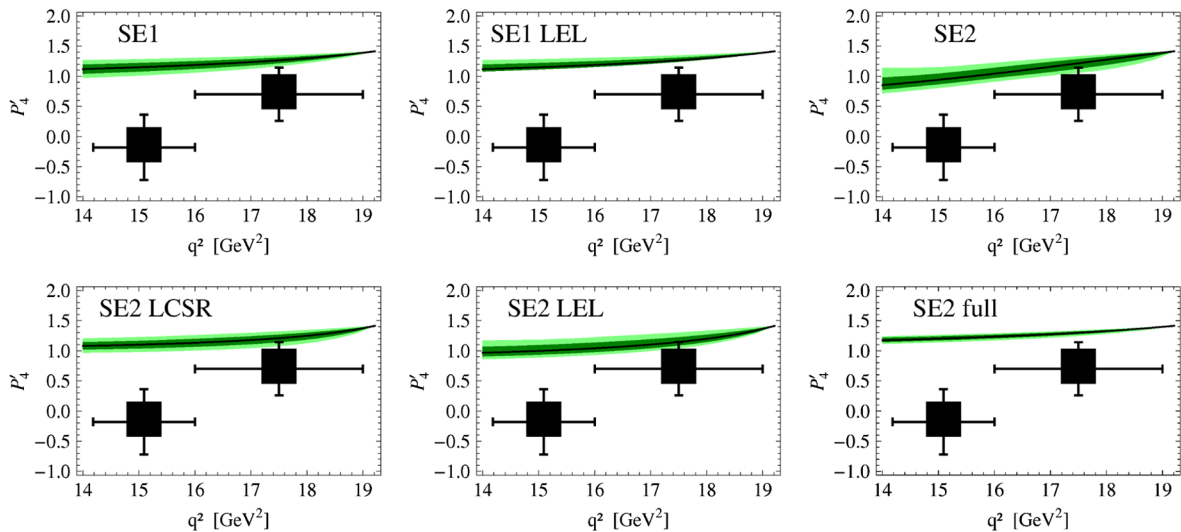


FIG. 5 (color online). Current data on  $P_4'$  by LHCb (black squares) together with the fit results; see Fig. 3.

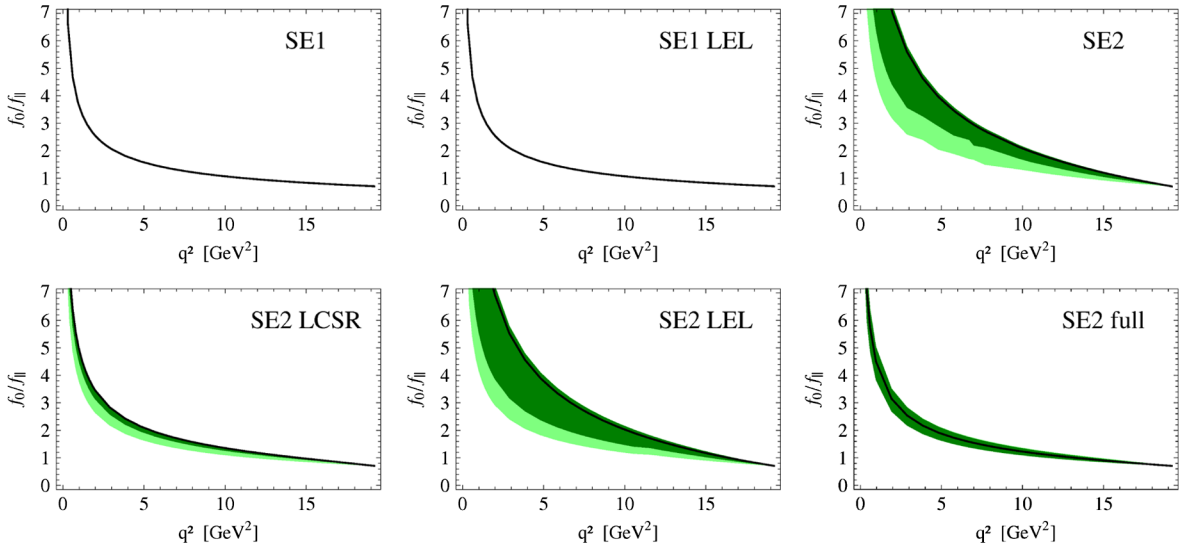


FIG. 6 (color online). Fit results as in Fig. 3 for  $f_0/f_{\parallel}$  in the full  $q^2$  range.  $f_0/f_{\parallel}$  is fixed within the SE1 parametrization.

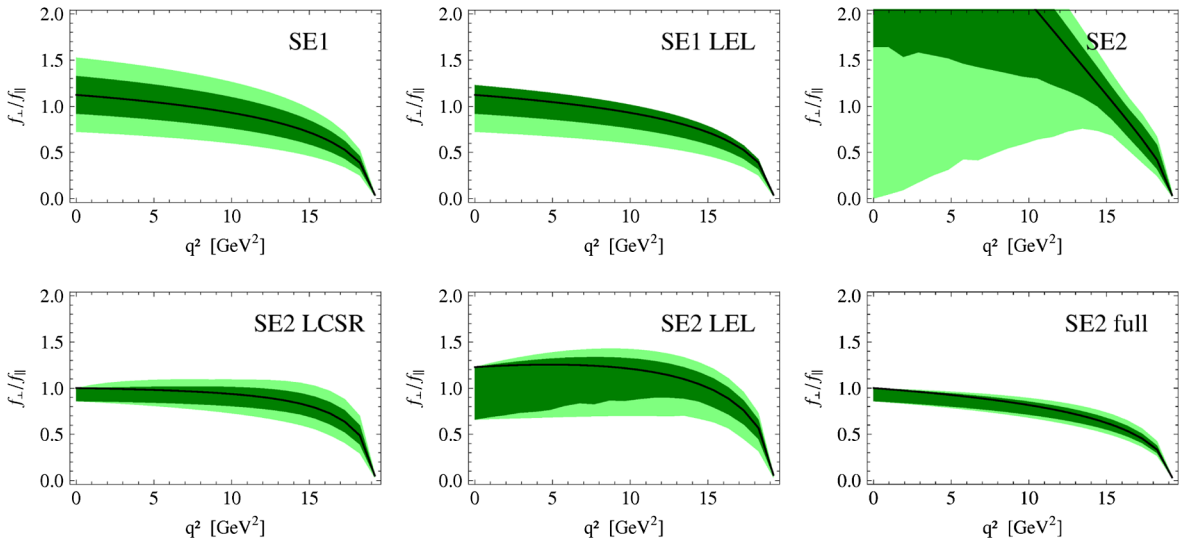


FIG. 7 (color online). Fit results as in Fig. 3 for  $f_{\perp}/f_{\parallel}$  for the full  $q^2$  range.

Finally, we compare predictions for  $V/A_1$  and  $f_0/f_{\parallel}$  in Fig. 10. Shown are recent lattice findings [15] (blue data points), the LCSR ratios Eq. (33) (red points) and the results from the fit to  $B \rightarrow K^* \ell^+ \ell^-$  data including LEL input in SE2 with the (68%) 95% C.L. regions shown as (dark green) light green bands. We observe, at this still quite early stage, consistency between the determinations at most  $q^2$  values. The largest discrepancies exist in  $V/A_1$  ( $2\sigma$ ) and at  $q^2 = 15.64 \text{ GeV}^2$  in  $f_0/f_{\parallel}$  ( $3\sigma$ ) between the lattice [15] and the SE2 LEL fit. Note that the lattice results for  $V/A_1$  shown are in agreement with previous ones for  $T_1/T_2$  [13,14] and the lowest order IWR, Eq. (31). In particular,  $R \gtrsim 1$ . The SE2 LEL fit exhibits a  $1.8\sigma$  discrepancy between LCSR results Eq. (33) and  $A_2(0)/A_1(0)$ ; see Table III.

In Fig. 11 we aim to predict the form factors themselves. Shown are predictions for  $V$ ,  $A_1$ ,  $A_2$  and

$f_0$  in the SE2 full fit, including form factors from the lattice [15] (blue data points) which fix the normalization. The LCSR predictions for form factors [10] (red hatched region) are not included in the fit. In all cases they exhibit very good agreement with the outcome of the full fit.

## V. PREDICTIONS IN SM AND BEYOND

We use the fit results for the form factor ratios from the previous section to obtain predictions for  $B \rightarrow K^* \ell^+ \ell^-$  observables. Specifically, we predict the forward-backward asymmetry  $A_{\text{FB}}$  and the angular observable  $P'_5$  [24,35] in the SM at low recoil. Up to the corrections indicated in Eq. (1), locally, they can be written as (see [25] and Appendix A)

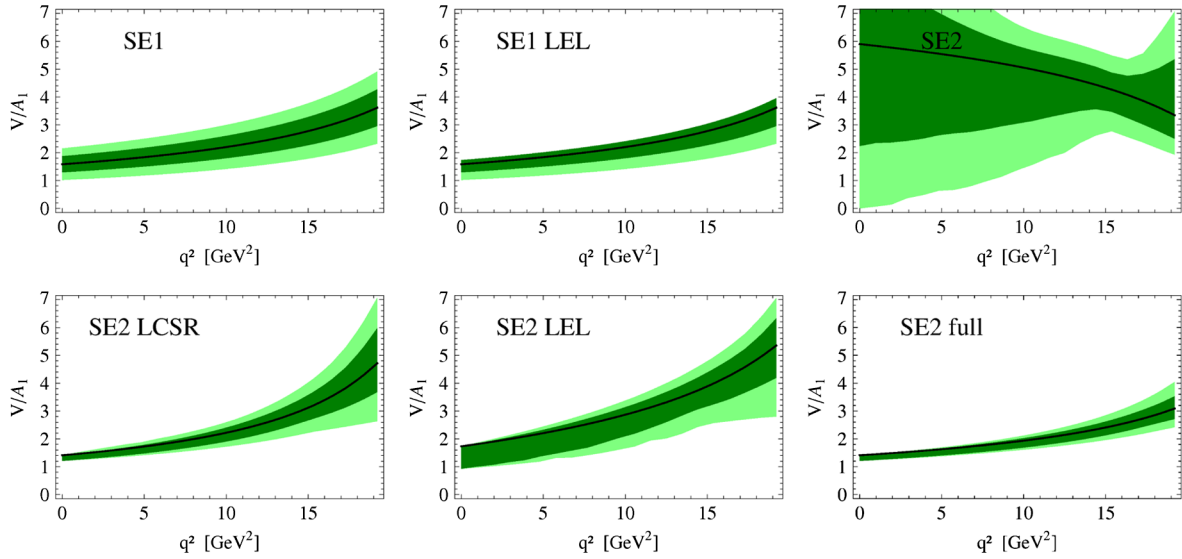


FIG. 8 (color online). Fit results as in Fig. 3 for  $V/A_1$  for the full  $q^2$  range.

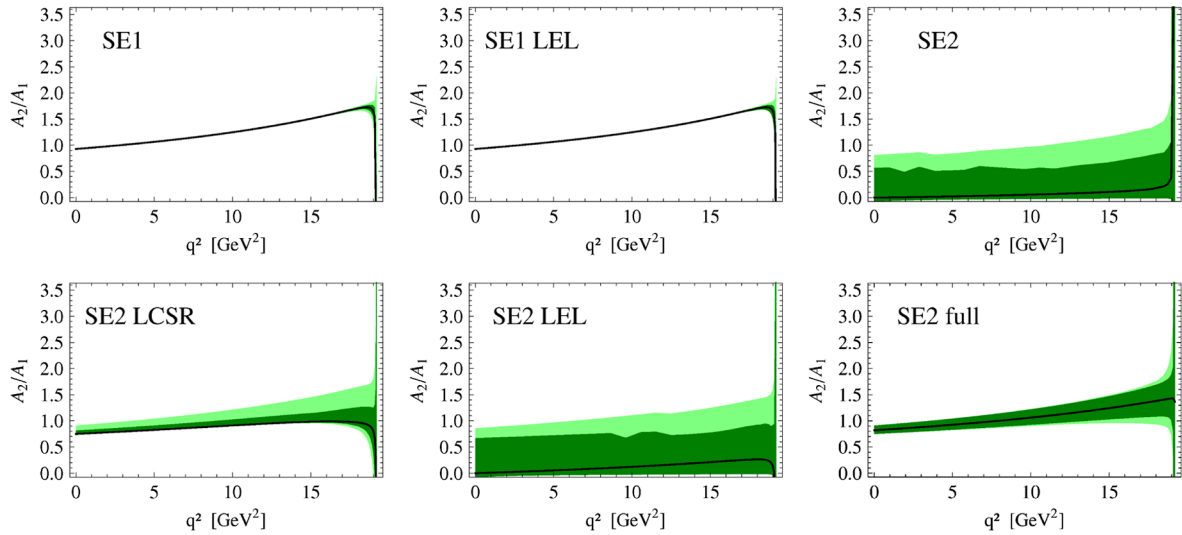


FIG. 9 (color online). Fit results as in Fig. 3 for  $A_2/A_1$  in the full  $q^2$  range.  $A_2/A_1$  is fixed within the SE1 parametrization.

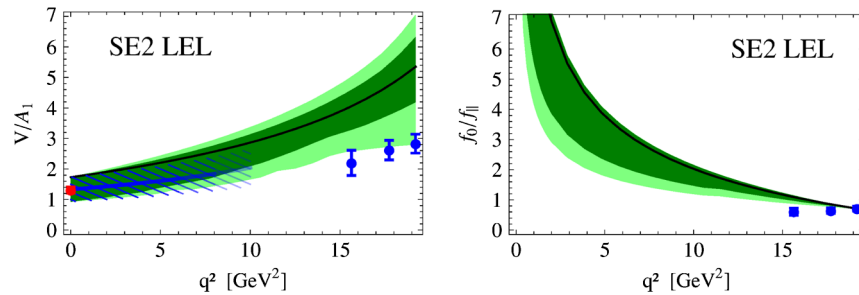


FIG. 10 (color online).  $V/A_1$  (left-handed plot) and  $f_0/f_{\parallel}$  (right-handed plot) from a fit to data including LEL in SE2 with 68% and 95% C.L. regions shown as dark green and light green bands, respectively. Also shown are lattice results [15] (blue data points), the LCSR ratio Eq. (33) (red point) and the LEL relation Eq. (27) (blue hatched band).

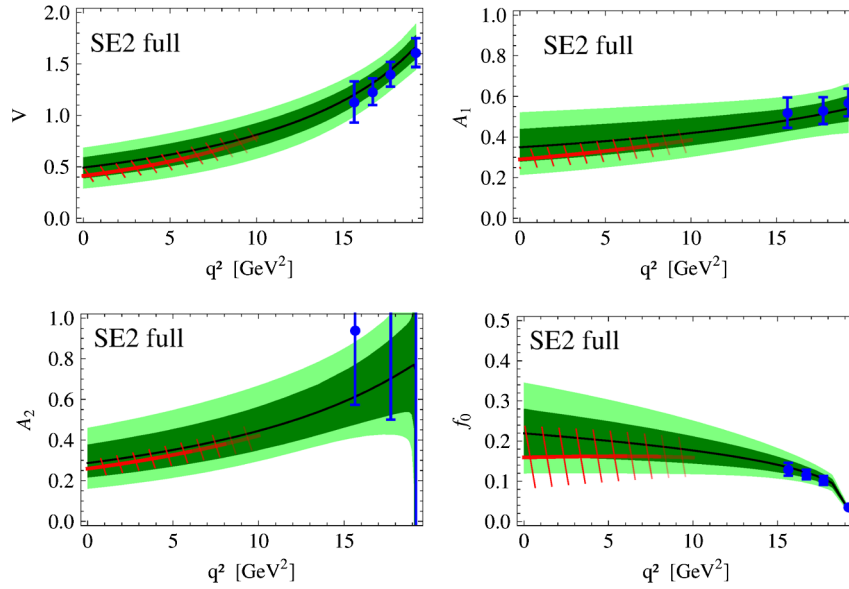


FIG. 11 (color online). Form factors in the SE2 full fit scenario, where in addition to the data and the LCSR ratio Eq. (33) the lattice results [15] (blue data points) have been taken into account for  $V$ ,  $A_1$  and  $A_2$ . The LCSR predictions for form factors [10] (red hatched region) are not included in the fit and are shown for comparison only. The (dark green) light green bands denote the (68%) 95% C.L. regions. The solid black curve corresponds to the best fit result.

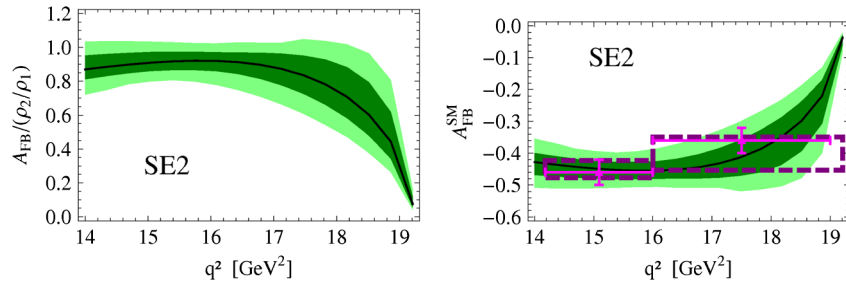


FIG. 12 (color online).  $A_{\text{FB}}/(\rho_2/\rho_1)$  (left-handed plot) and  $A_{\text{FB}}^{\text{SM}}$  (right-handed plot) at low recoil from fit to data in SE2. The (68%) 95% C.L. regions are shown in (dark green) light green. The dashed (purple) boxes denote the  $1\sigma$  SM bins. The data points (magenta) correspond to the experimental world average; see Table IV.

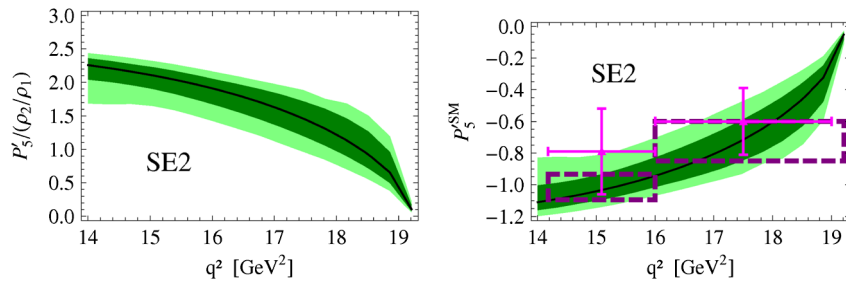


FIG. 13 (color online).  $P'_5/(\rho_2/\rho_1)$  (left-handed plot) and  $P_5^{\text{SM}}$  (right-handed plot) at low recoil from fit to data in SE2. The (68%) 95% C.L. regions are shown in (dark green) light green. The dashed (purple) boxes denote the  $1\sigma$  SM bins. The data points (magenta) correspond to the experimental world average; see Table V.

TABLE IV. Experimental world average [1–5,67] of  $A_{\text{FB}}$  at low recoil and corresponding SM predictions from [29] and our fits in different parameterizations. The global sign of the  $A_{\text{FB}}$  data has been adjusted to match the conventions as in Ref. [29]. There are no high luminosity data available for  $A_{\text{FB}}$  in the full low recoil bin.

$q^2$ [GeV <sup>2</sup> ]	Data	SM [29]	SM SE1	SM SE1 LEL	SM SE2	SM SE2 LCSR	SM SE2 LEL	SM SE2 full
[14.18, 16]	$-0.46 \pm 0.04$	$-0.44^{+0.07}_{-0.07}$	$-0.48^{+0.05}_{-0.04}$	$-0.48^{+0.05}_{-0.02}$	$-0.45^{+0.02}_{-0.03}$	$-0.46^{+0.04}_{-0.03}$	$-0.44^{+0.03}_{-0.03}$	$-0.42^{+0.00}_{-0.03}$
[16, $q_{\text{max}}^2$ ]	$-0.36 \pm 0.04$	$-0.38^{+0.06}_{-0.07}$	$-0.40^{+0.06}_{-0.05}$	$-0.40^{+0.06}_{-0.03}$	$-0.40^{+0.05}_{-0.05}$	$-0.43^{+0.05}_{-0.05}$	$-0.45^{+0.05}_{-0.03}$	$-0.35^{+0.03}_{-0.00}$
[14.18, $q_{\text{max}}^2$ ]			$-0.43^{+0.06}_{-0.04}$	$-0.43^{+0.06}_{-0.02}$	$-0.42^{+0.03}_{-0.03}$	$-0.45^{+0.05}_{-0.04}$	$-0.44^{+0.03}_{-0.03}$	$-0.38^{+0.03}_{-0.03}$

TABLE V. Preliminary LHCb data [6] of  $P'_5$  at low recoil and corresponding SM predictions from [24] with errors added in quadrature and our fits in different parameterizations. There are no data available for  $P'_5$  in the full low recoil bin.

$q^2$ [GeV <sup>2</sup> ]	Data	SM [24]	SM SE1	SM SE1 LEL	SM SE2	SM SE2 LCSR	SM SE2 LEL	SM SE2 full
[14.18, 16]	$-0.79^{+0.27}_{-0.22}$	$-0.78^{+0.33}_{-0.36}$	$-0.81^{+0.11}_{-0.09}$	$-0.81^{+0.11}_{-0.05}$	$-1.03^{+0.10}_{-0.06}$	$-0.87^{+0.08}_{-0.07}$	$-0.98^{+0.10}_{-0.06}$	$-0.73^{+0.06}_{-0.05}$
[16, $q_{\text{max}}^2$ ]	$-0.60^{+0.21}_{-0.18}$	$-0.60^{+0.28}_{-0.37}$	$-0.62^{+0.09}_{-0.09}$	$-0.62^{+0.09}_{-0.05}$	$-0.73^{+0.13}_{-0.12}$	$-0.73^{+0.10}_{-0.09}$	$-0.81^{+0.12}_{-0.07}$	$-0.55^{+0.05}_{-0.05}$
[14.18, $q_{\text{max}}^2$ ]			$-0.70^{+0.10}_{-0.09}$	$-0.70^{+0.10}_{-0.05}$	$-0.88^{+0.13}_{-0.08}$	$-0.80^{+0.09}_{-0.08}$	$-0.89^{+0.12}_{-0.07}$	$-0.64^{+0.06}_{-0.05}$

$$A_{\text{FB}}(q^2) = \frac{\rho_2(q^2)}{\rho_1(q^2)} \cdot \frac{3f_{\parallel}(q^2)f_{\perp}(q^2)}{f_0^2(q^2) + f_{\perp}^2(q^2) + f_{\parallel}^2(q^2)}, \quad (46)$$

$$P'_5(q^2) = \frac{\rho_2(q^2)}{\rho_1(q^2)} \cdot \frac{2\sqrt{2}f_{\perp}(q^2)}{\sqrt{f_{\parallel}^2(q^2) + f_{\perp}^2(q^2)}}, \quad (47)$$

where

$$\begin{aligned} \rho_1(q^2) &= \frac{1}{2} (|C^R(q^2)|^2 + |C^L(q^2)|^2), \\ \rho_2(q^2) &= \frac{1}{4} (|C^R(q^2)|^2 - |C^L(q^2)|^2). \end{aligned} \quad (48)$$

The factorization into short-distance coefficients and form factor ones is again manifest. Importantly, only form factor ratios enter. The ranges are  $-3/4 \leq A_{\text{FB}} \leq 3/4$  and  $-\sqrt{2} \leq P'_5 \leq \sqrt{2}$ .

In Figs. 12 and 13 (left-handed plots) we show the predictions of the fit for the purely form factor-dependent factors  $A_{\text{FB}}/(\rho_2/\rho_1)$  and  $P'_5/(\rho_2/\rho_1)$ , respectively. Also shown in the figures (right-handed plots) are the resulting SM predictions taking the short-distance factors  $\rho_{1,2}$  in the SM from [25] with parameters as in [29]. Here, SE2 has been employed. Fits to the other parametrizations give similar results at low recoil and are not shown. In Tables IV and V we further give  $q^2$ -binned values of  $A_{\text{FB}}^{\text{SM}}$  and  $P_5^{\text{SM}}$ , respectively, obtained using the binning procedure described in Sec. II A.

For both  $A_{\text{FB}}$  and  $P'_5$  we find that the low recoil data are in good agreement with the corresponding SM predictions resulting from the data-extracted form factor ratios. The SM predictions at low recoil are stable under change of the fit parameterization, apart from the first  $P'_5$  bin which exhibits a  $2.5\sigma$  tension between SE2 and SE2 full, and are consistent with Refs. [24,29]. We recall from Sec. IV C that

we consider the fit scenarios SE2, SE2 LEL and SE2 LCSR as best suited presently for low recoil phenomenology. The SE2 full fit, on the other hand, demonstrates the future potential of combining data with LCSR and precision lattice input.

The theoretical uncertainties from the fit output in Figs. 12 and 13 and Tables IV and V correspond to form factor ones only. The uncertainties from the SM value of  $\rho_2/\rho_1$  are subleading, about 2% [25]. The resulting combined uncertainties for  $A_{\text{FB}}$  and  $P'_5$  are smaller than the ones obtained previously [24,29] and can be further reduced by experimental measurements. Note that while  $F_L, A_T^{(2)}$  and  $P'_4$  are protected from leading  $c\bar{c}$  contributions [34], such effects need to be considered in more detail in  $A_{\text{FB}}$  and  $P'_5$  once data are more precise.

## VI. CONCLUSIONS

Our main conclusion is that QCD input to flavor observables can be model-independently extracted from rare decay data and fed back towards improving the SM predictions. This happens twofold, indirectly by providing benchmarks for nonperturbative methods and directly as we demonstrated for  $A_{\text{FB}}$  and  $P'_5$ ; see Figs. 12 and 13, respectively.

While the first point has been made previously [30] here we significantly improved on the latter analysis by using more detailed fits. Our results, based on  $V-A$  operators only, are summarized in Sec. IV C. We stress that fits at low recoil provide quite parameterization-independent experimental information on form factor ratios in this region. This is useful for direct comparison with lattice predictions in particular. The more ambitious extrapolations to the whole kinematic range are more sensitive to the parameterization and in particular require some large recoil input, taken here from LCSR, Eq. (33), or heavy quark large energy symmetries, Eq. (27).

Overall, there is consistency between determinations of form factor ratios based on  $B \rightarrow K^* \ell^+ \ell^-$  data, lattice QCD, heavy quark and large energy symmetries and LCSR at present at the exception of a few outliers; see Fig. 10. It is interesting to follow up on whether these different methods in the future converge or exhibit a conflict. Either way will be informative for flavor physics and QCD calculations.

We consider the fit scenarios SE2, SE2 LEL and SE2 LCSR as best suited presently for low recoil phenomenology. The SE2 full fit demonstrates the future potential of a combined fit including LCSR and precision lattice results.

Already with present data the SM predictions of NP-sensitive observables  $A_{\text{FB}}$  and  $P'_5$  from fitted form factor ratios improve on existing estimates; see Table IV and V, respectively. Presently, there is good agreement with the SM in these observables at low recoil. This requires, at least within the SM basis of  $|\Delta B| = |\Delta S| = 1$  operators used in this work, that NP contributions to semileptonic short-distance coefficients are to be small. Explanations of the current anomaly in  $P'_5$  data at large recoil [6] based on order one NP predominantly in the Wilson coefficient  $\mathcal{C}_9$  alone [68] are therefore strongly disfavored, in agreement with the findings of [69,70].

We encourage further experimental investigations to shed light on the  $\sim 2\sigma$  discrepancy in  $P'_4$ , which within the OPE cannot be explained; see Fig. 5 and also [69]. We stress that higher  $c\bar{c}$  resonances at low recoil as observed recently in  $B^+ \rightarrow K^+ \mu^+ \mu^-$  [71] are expected, e.g., [72–74]. The OPE can, generally, be expected to work better for larger binning. Whether this is the case with present data, or the general performance of the OPE could be accessed using different binnings, including the full low recoil one, and with dedicated observables, such as  $H_T^{(1)}$  and  $H_T^{(2)}/H_T^{(3)}$  [25], which quantify breakings of the universality feature of the OPE, Eq. (1).

## ACKNOWLEDGMENTS

R.Z. gratefully acknowledges the support of an advanced STFC fellowship. We are grateful to Jerome Charles, Einan Gardi and James Lyon for useful discussions and to Danny van Dyk for providing numerical values of SM Wilson coefficients as in [29] and comments on the manuscript. We are happy to thank Matthew Wingate for sharing preliminary lattice results with us. This work is supported by the Deutsche Forschungsgemeinschaft (DFG) within research unit FOR 1873.

## APPENDIX A: OBSERVABLES FROM ANGULAR COEFFICIENTS

The  $B \rightarrow K^* \ell^+ \ell^-$  observables used in this work can be written in terms of the angular coefficients  $J_k = J_k(q^2)$  as

$$\begin{aligned} \frac{d\Gamma}{dq^2} &= \frac{4}{3}(4J_{2s} - J_{2c}), & A_{\text{FB}} &= \frac{J_6}{d\Gamma/dq^2}, \\ F_L &= -\frac{4}{3} \frac{J_{2c}}{d\Gamma/dq^2}, & A_T^{(2)} &= \frac{1}{2} \frac{J_3}{J_{2s}}, \\ P'_4 &= \frac{J_4}{\sqrt{-J_{2s}J_{2c}}}, & P'_5 &= \frac{J_5}{2\sqrt{-J_{2s}J_{2c}}}. \end{aligned} \quad (\text{A1})$$

The  $J_k$  are related to the transversity amplitudes  $f_{0,\parallel,\perp}$  at low recoil as follows:

$$\begin{aligned} -\frac{4}{3}J_{2c} &= 2\rho_1 f_0^2, & \frac{4}{3}[2J_{2s} + J_3] &= 2\rho_1 f_\perp^2, \\ \frac{4}{3}[2J_{2s} - J_3] &= 2\rho_1 f_\parallel^2, & \frac{\sqrt{32}}{3}J_4 &= 2\rho_1 f_0 f_\parallel, \\ \frac{\sqrt{8}}{3}J_5 &= 4\rho_2 f_0 f_\perp, & \frac{2}{3}J_6 &= 4\rho_2 f_\parallel f_\perp. \end{aligned} \quad (\text{A2})$$

The short-distance coefficients  $\rho_{1,2}$  are given in Eq. (48). We neglect lepton masses; hence the formulae do not apply to tau leptons.  $CP$  averaging and SM operator basis is understood. For further details on the full angular distribution, see, e.g., [29].

## APPENDIX B: DEFINITIONS

### 1. The $B \rightarrow K^*$ form factors

The (axial-)vector and tensor form factors are defined as follows:

$$\begin{aligned} (f_\lambda^T)^\mu &= \langle K^*(p, \eta(\lambda)) | \bar{s} i q_\nu \sigma^{\mu\nu} (a + \gamma_5) b | \bar{B}(p_B) \rangle \\ &= a P_1^\mu T_1(q^2) + P_2^\mu T_2(q^2) + P_3^\mu T_3(q^2), \\ T_1(0) &= T_2(0), \\ (f_\lambda^V)^\mu &= \langle K^*(p, \eta(\lambda)) | \bar{s} \gamma^\mu (a - \gamma_5) b | \bar{B}(p_B) \rangle \\ &= a P_1^\mu \mathcal{V}_1(q^2) + P_2^\mu \mathcal{V}_2(q^2) + P_3^\mu \mathcal{V}_3(q^2) + P_P^\mu \mathcal{V}_P(\mathbf{q}^2), \end{aligned}$$

where  $a$  is a constant separating the parity-violating and parity-conserving parts and  $\mathcal{V}_1$  and  $\mathcal{A}_{0,2,3}$  are given by

$$\begin{aligned} \mathcal{V}_P(q^2) &= \frac{-2m_{K^*}}{q^2} A_0(q^2), & \mathcal{V}_1(q^2) &= \frac{-V(q^2)}{m_B + m_{K^*}}, \\ \mathcal{V}_2(q^2) &= \frac{-A_1(q^2)}{m_B - m_{K^*}}, \\ \mathcal{V}_3(q^2) &= \left( \frac{m_B + m_{K^*}}{q^2} A_1(q^2) - \frac{m_B - m_{K^*}}{q^2} A_2(q^2) \right) \\ &\equiv \frac{2m_{K^*}}{q^2} A_3(q^2). \end{aligned} \quad (\text{B2})$$

The relation  $A_3(0) = A_0(0)$  assures finite matrix elements at  $q^2 = 0$  and  $A_0(0) \neq 0$  corresponds to the pseudoscalar form factor. The Lorentz structures  $P_i^\mu$  are

given by

$$\begin{aligned} P_P^\mu &= i(\eta^* \cdot q)q^\mu, & P_1^\mu &= 2\epsilon^{\mu\alpha\beta\gamma}\eta^{*\alpha}p^\beta q^\gamma, \\ P_2^\mu &= i\{(m_B^2 - m_{K^*}^2)\eta^{*\mu} - (\eta^* \cdot q)(p + p_B)^\mu\}, \\ P_3^\mu &= i(\eta^* \cdot q)\left\{q^\mu - \frac{q^2}{m_B^2 - m_{K^*}^2}(p + p_B)^\mu\right\}, \end{aligned} \quad (\text{B3})$$

$$\begin{aligned} q_\mu \langle K^*(p, \eta(\lambda)) | \bar{s}\gamma^\mu(-\gamma_5)b | \bar{B}(p_B) \rangle &= (m_s + m_b) \langle K^*(p, \eta(\lambda)) | \bar{s}\gamma_5 b | \bar{B}(p_B) \rangle \\ \Rightarrow \langle K^*(p, \eta(\lambda)) | \bar{s}\gamma_5 b | \bar{B}(p_B) \rangle &= \left(\frac{P_P \cdot q}{m_s + m_b}\right) \mathcal{V}_P(q^2) = \left(\frac{2m_{K^*}(\eta^* \cdot q)}{i(m_s + m_b)}\right) A_0(q^2), \end{aligned} \quad (\text{B4})$$

is at the origin of the subscript  $P$ . The reason for not choosing 0 as a subscript is to avoid confusion with the zero helicity label. We observe that the pole  $1/q^2$  disappears as it should.

For the reader's convenience we give here the relations between the  $\mathcal{D}_{1,2,3,P}$  (12) and  $d, d_{1,\pm}$  as used in [26]:

$$\begin{aligned} \mathcal{D}_1 &= 2d, \\ \mathcal{D}_3 &= \frac{-2}{q^2}(d_1 + d_+(m_B^2 - m_{K^*}^2)), \\ \mathcal{D}_2 &= \frac{+2d_1}{m_B^2 - m_{K^*}^2}, \\ \mathcal{D}_P &= \frac{+2}{q^2}(d_1 + d_-q^2 + d_+(m_B^2 - m_{K^*}^2)), \end{aligned} \quad (\text{B5})$$

where  $\mathcal{D}_P + \mathcal{D}_3 = +2d_-$  is the combination that is free of a pole of the form  $1/q^2$ .

The leading heavy quark form factors  $\mathcal{D}_k^{(0)}$ ,  $k = 1, 2, 3, P$  obtained by replacing the QCD field  $b$  by the corresponding heavy quark field are defined using an identical Lorentz decomposition as the QCD form factors  $\mathcal{D}_k$ , Eq. (12).

## 2. The $B \rightarrow K$ form factors

For completeness we give the definition of the  $B \rightarrow K$  form factors as well as the derivative form factors:

$$\begin{aligned} \langle K(p) | \bar{s}i q_\nu \sigma^{\mu\nu} b | \bar{B}(p_B) \rangle &= P_T^\mu f_T(q^2), \\ \langle K(p) | \bar{s}\gamma^\mu b | \bar{B}(p_B) \rangle &= P_T^\mu v_T + q^\mu v_s, \\ \langle K(p) | (2i\vec{D})^\mu | \bar{B}(p_B) \rangle &= P_T^\mu \mathcal{D}_T(q^2) + q^\mu \mathcal{D}_s(q^2), \end{aligned} \quad (\text{B6})$$

where

$$P_T^\mu = \frac{1}{m_B + m_K} \{(m_B^2 - m_K^2)q^\mu - q^2(p + p_B)^\mu\} \quad (\text{B7})$$

and  $v_{s,T}$  relate to the standard form factors  $f_{0,+}$  as follows:

with Bjorken and Drell convention for the Levi-Civita tensor  $\epsilon_{0123} = +1$ . The reason for the mismatch between the indices between  $\mathcal{A}$  and  $A$  is due to the fact that the original nomenclature between the axial  $A_i$ - and tensor  $T_i$ -form factors is not coherent from the viewpoint of the Lorentz decomposition. Furthermore note that the following relation:

$$v_s = \frac{m_B^2 - m_K^2}{q^2} f_0(q^2), \quad v_T = \frac{-(m_B + m_K)}{q^2} f_+(q^2). \quad (\text{B8})$$

We note that  $f_0(0) = f_+(0)$  for the same reasons that  $A_0(0) = A_3(0)$  for the vector form factors. When applied to the e.o.m., the first equation in (11), one obtains two relations for the  $P_T^\mu$  and  $q^\mu$  directions:

$$\begin{aligned} f_T(q^2) &= -(m_s + m_b)v_T - \mathcal{D}_T(q^2), \\ 0 &= \left(\frac{q^2}{m_b + m_s} - (m_s + m_b)\right)v_s - \mathcal{D}_s(q^2). \end{aligned} \quad (\text{B9})$$

Adding these two, and using the standard form factors  $f_{0,+}$  one obtains

$$\begin{aligned} f_T(q^2) &= (m_B + m_K)(m_b + m_s) \\ &\times \left[ \frac{f_+(q^2) - f_0(q^2)}{q^2} + \frac{f_0(q^2)}{(m_b + m_s)^2} \right] \\ &- \left[ \mathcal{D}_T(q^2) + \frac{\mathcal{D}_s(q^2)}{m_B - m_K} \right], \end{aligned} \quad (\text{B10})$$

where both terms in square brackets are finite in the  $q^2 \rightarrow 0$  limit for the same reasons as for the vector form factors discussed below Eq. (17).

## 3. Subtracted form factors

Using  $A_3(0) = A_0(0)$  we write

$$\begin{aligned} \mathcal{D}_3(q^2) &= \frac{+c_3 A_3(0)}{q^2} + \bar{\mathcal{D}}_3(q^2), \\ \mathcal{D}_P(q^2) &= \frac{-c_3 A_3(0)}{q^2} + \bar{\mathcal{D}}_P(q^2), \end{aligned} \quad (\text{B11})$$

where  $\bar{\mathcal{D}}_{0,3}(q^2)$  are regular as  $q^2 \rightarrow 0$ . Defining  $\bar{A}_{0,3}(q^2) = A_{0,3}(q^2) - A_{0,3}(0)$  one obtains the expressions

$$T_3(q^2) = \frac{c_3}{q^2} \bar{A}_3(q^2) - \bar{\mathcal{D}}_3(q^2),$$

$$0 = \left( c_P A_0(q^2) - \frac{c_3}{q^2} \bar{A}_0(q^2) \right) - \bar{\mathcal{D}}_P(q^2). \quad (\text{B12})$$

These differ from Eqs. (15) by the fact that both terms on the right-hand side are separately regular.

### APPENDIX C: LCSR TREE-LEVEL ANALYSIS

We illustrate the power suppression of  $\mathcal{D}_{1,2,+}(0)$  as discussed in Sec. III B 1 through explicit LCSR results at tree level. Consider the following LCSR representation of the form factors:

$$c_1 \rho_V(s, 0) = \frac{3m_b^3}{2s^3} (2f_{K^*}^\perp m_b (s - m_b^2) + f_{K^*}^\parallel m_{K^*} [m_b^2 - (s - m_b^2)]) + \mathcal{O}(\alpha_s, \text{higher twist}),$$

$$c_2 \rho_{A_1}(s, 0) = \frac{3m_b^3}{2s^3} (2f_{K^*}^\perp m_b (s - m_b^2) + f_{K^*}^\parallel m_{K^*} [m_b^2 + (s - m_b^2)^2/s]) + \mathcal{O}(\alpha_s, \text{higher twist}). \quad (\text{C2})$$

The symbols  $f_{K^*}^{\perp,\parallel}$  denote the longitudinal and transversal decay constant of the  $K^*$  meson, respectively. Here, the twist-2 and twist-3 parts correspond to  $f_{K^*}^{\perp,\parallel}$ , respectively. Using (20) this implies

$$\sqrt{2} \rho_{\mathcal{D}_+}(s, 0) \stackrel{(14)}{=} (c_1 \rho_V(s, 0) - c_2 \rho_{A_1}(s, 0)) \stackrel{(C.2)}{=} -\frac{3m_b^3}{2s^3} f_{K^*}^\parallel m_{K^*} (s - m_b^2) (2 - m_b^2/s) + \mathcal{O}(\alpha_s, \text{higher twist}). \quad (\text{C3})$$

We note that the leading term in  $1/m_b$  cancels as anticipated. The scaling  $\mathcal{D}_+(0)/V(0) \propto \mathcal{D}_+(0)/A_1(0) \propto \Lambda/m_b$  is now almost manifest as  $(s - m_b^2) \sim \mathcal{O}(\Lambda m_b)$  at best at the upper boundary of integration in (C1). The exponential factor does not change anything as the scaling of the Borel parameter (C4) is arranged to keep it finite in the  $m_b \rightarrow \infty$  limit. Let us be more specific and implement the heavy quark limit [52] which amounts to the replacements

$$m_B \rightarrow m_b + \bar{\Lambda}, \quad s_0 \rightarrow m_b^2 + 2m_b \omega_0, \quad M^2 \rightarrow 2m_b \tau. \quad (\text{C4})$$

Here,  $\bar{\Lambda}$ ,  $\omega_0$  and  $\tau$  are all hadronic quantities of the order of  $\Lambda$  out of which  $\bar{\Lambda}$  is known rather precisely through the experimental value of  $m_B$ . Using  $f_B \rightarrow (f_B)_{\text{stat}} m_b^{-1/2}$ , e.g., [75], we obtain

$$c_1 V(0) \simeq c_2 A_1(0) \simeq \frac{(3f_{K^*}^\parallel m_{K^*} \omega_0 + 12f_{K^*}^\perp \omega_0^2 \langle z \rangle)}{(f_B)_{\text{stat}} m_b^{3/2}}, \quad \sqrt{2} \mathcal{D}_+(0) \simeq \frac{-6f_{K^*}^\parallel m_{K^*} \omega_0^2 \langle z \rangle}{(f_B)_{\text{stat}} m_b^{5/2}}, \quad (\text{C5})$$

where  $\simeq$  stands for the above mentioned higher twist  $\mathcal{O}(\alpha_s)$  and, by now, also  $\mathcal{O}(\Lambda/m_b)$  corrections. Furthermore  $\langle f(z) \rangle = \int_0^1 e^{\frac{(\bar{\Lambda} - \omega_0 z)}{\tau}} f(z) dz$  is a quantity which is  $\mathcal{O}(1)$  as it has no  $m_b$  dependence.

The power suppression of the  $\mathcal{D}_{1,2}(0)$  with respect to the standard form factors at  $\mathcal{O}(\alpha_s^0)$  follows analogously from

$$\rho_{T_1}(s, 0) = 3m_b^3 / (2s^3) (2f_{K^*}^\perp m_b (s - m_b^2) + f_{K^*}^\parallel m_{K^*} m_b^2) + \mathcal{O}(\alpha_s, \text{higher twist}) \quad (\text{C6})$$

together with Eqs. (C2) and (14).

$$F(q^2) = \frac{1}{m_B^2 f_B} \int_{m_b^2}^{s_0^F} ds e^{(m_b^2 - s)/M_F^2} \rho_F(s, q^2),$$

$$F \in \{T_{1,2}, V, A_1, \mathcal{D}_{1,2}, \dots\}, \quad (\text{C1})$$

where  $M_F^2$  and  $s_0^F$  are in general form-factor-dependent Borel parameters and continuum thresholds, respectively. Note that the decay constant  $f_B$  has to be taken from a QCD sum rule to the same  $\mathcal{O}(\alpha_s)$  accuracy in order to cancel radiative corrections appropriately; see e.g., [10]. To  $\mathcal{O}(\alpha_s^0)$  up to twist-3 and  $m_s = 0$  and at  $q^2 = 0$  one obtains, using for instance the results given in [10],

- [1] S. Akar (BABAR Collaboration), in Proceedings of the Lake Louise Winter Institute, Canada, 2012 (unpublished).
- [2] CDF Note No. 10894, 2012, <http://www-cdf.fnal.gov/physics/new/bottom/>.
- [3] R. Aaij *et al.* (LHCb Collaboration), *J. High Energy Phys.* **08** (2013) 131.
- [4] ATLAS Collaboration, Report No. ATLAS-CONF-2013-038, <http://cds.cern.ch/record/1537961>.
- [5] S. Chatrchyan *et al.* (CMS Collaboration), *Phys. Lett. B* **727**, 77 (2013).
- [6] R. Aaij *et al.* (LHCb Collaboration), *Phys. Rev. Lett.* **111**, 191801 (2013).
- [7] A. Faessler, T. Gutsche, M. A. Ivanov, J. G. Korner, and V. E. Lyubovitskij, *Eur. Phys. J. direct C* **4**, 1 (2002).
- [8] D. Ebert, R. N. Faustov, and V. O. Galkin, *Phys. Rev. D* **82**, 034032 (2010).
- [9] P. Ball and V. M. Braun, *Phys. Rev. D* **58**, 094016 (1998).
- [10] P. Ball and R. Zwicky, *Phys. Rev. D* **71**, 014029 (2005).
- [11] A. Khodjamirian, T. Mannel, and N. Offen, *Phys. Rev. D* **75**, 054013 (2007).
- [12] P. Ball and R. Zwicky, *Phys. Lett. B* **633**, 289 (2006).
- [13] D. Becirevic, V. Lubicz, and F. Mescia, *Nucl. Phys. B* **769**, 31 (2007).
- [14] Z. Liu, S. Meinel, A. Hart, R. R. Horgan, E. H. Muller, and M. Wingate, [arXiv:1101.2726](https://arxiv.org/abs/1101.2726).
- [15] R. R. Horgan, Z. Liu, S. Meinel, and M. Wingate, [arXiv:1310.3722](https://arxiv.org/abs/1310.3722).
- [16] F. Krüger and J. Matias, *Phys. Rev. D* **71**, 094009 (2005).
- [17] C. Bobeth, G. Hiller, and G. Piranishvili, *J. High Energy Phys.* **07** (2008) 106.
- [18] U. Egede, T. Hurth, J. Matias, M. Ramon, and W. Reece, *J. High Energy Phys.* **11** (2008) 032.
- [19] W. Altmannshofer, P. Ball, A. Bharucha, A. J. Buras, D. M. Straub, and M. Wick, *J. High Energy Phys.* **01** (2009) 019.
- [20] E. Lunghi and A. Soni, *J. High Energy Phys.* **11** (2010) 121.
- [21] A. K. Alok, A. Datta, A. Dighe, M. Duraisamy, D. Ghosh, and D. London, *J. High Energy Phys.* **11** (2011) 121.
- [22] D. Becirevic and E. Schneider, *Nucl. Phys.* **B854**, 321 (2012).
- [23] D. Das and R. Sinha, *Phys. Rev. D* **86**, 056006 (2012).
- [24] S. Descotes-Genon, T. Hurth, J. Matias, and J. Virto, *J. High Energy Phys.* **05** (2013) 137.
- [25] C. Bobeth, G. Hiller, and D. van Dyk, *J. High Energy Phys.* **07** (2010) 098.
- [26] B. Grinstein and D. Pirjol, *Phys. Rev. D* **70**, 114005 (2004).
- [27] M. Beylich, G. Buchalla, and T. Feldmann, *Eur. Phys. J. C* **71**, 1635 (2011).
- [28] B. Grinstein and D. Pirjol, *Phys. Lett. B* **533**, 8 (2002).
- [29] C. Bobeth, G. Hiller, and D. van Dyk, *Phys. Rev. D* **87**, 034016 (2013).
- [30] C. Hambroek and G. Hiller, *Phys. Rev. Lett.* **109**, 091802 (2012).
- [31] F. Beaujean, C. Bobeth, D. van Dyk, and C. Wacker, *J. High Energy Phys.* **08** (2012) 030.
- [32] R. Aaij *et al.* (LHCb Collaboration), *Eur. Phys. J. C* **73**, 2373 (2013).
- [33] T. Aushev *et al.*, [arXiv:1002.5012](https://arxiv.org/abs/1002.5012).
- [34] G. Hiller and R. Zwicky, [arXiv:1312.1923](https://arxiv.org/abs/1312.1923).
- [35] S. Descotes-Genon, J. Matias, M. Ramon, and J. Virto, *J. High Energy Phys.* **01** (2013) 048.
- [36] R. Zwicky, [arXiv:1309.7802](https://arxiv.org/abs/1309.7802).
- [37] N. Isgur and M. B. Wise, *Phys. Rev. D* **42**, 2388 (1990).
- [38] D. Pirjol and I. W. Stewart, *Proceedings of the Second Conference on Flavor Physics and CP Violation (FPCP 2003)*, Paris, France, eConf C030603, MEC04 (2003).
- [39] G. Burdman and J. F. Donoghue, *Phys. Lett. B* **270**, 55 (1991).
- [40] J. Charles, A. Le Yaouanc, L. Oliver, O. Pène, and J.-C. Raynal, *Phys. Rev. D* **60**, 014001 (1999).
- [41] M. Beneke and T. Feldmann, *Nucl. Phys.* **B592**, 3 (2001).
- [42] C. W. Bauer, S. Fleming, D. Pirjol, and I. W. Stewart, *Phys. Rev. D* **63**, 114020 (2001).
- [43] G. Burdman and G. Hiller, *Phys. Rev. D* **63**, 113008 (2001).
- [44] M. Beneke and D. Yang, *Nucl. Phys.* **B736**, 34 (2006).
- [45] D. Atwood, M. Gronau, and A. Soni, *Phys. Rev. Lett.* **79**, 185 (1997).
- [46] F. Muheim, Y. Xie, and R. Zwicky, *Phys. Lett. B* **664**, 174 (2008).
- [47] D. Becirevic, E. Kou, A. Le Yaouanc, and A. Tayduganov, *J. High Energy Phys.* **08** (2012) 090.
- [48] S. Jäger and J. Martin Camalich, *J. High Energy Phys.* **05** (2013) 043.
- [49] M. Dimou, J. Lyon, and R. Zwicky, *Phys. Rev. D* **87**, 074008 (2013).
- [50] J. Lyon and R. Zwicky, *Phys. Rev. D* **88**, 094004 (2013).
- [51] P. Ball and R. Zwicky, *Phys. Rev. D* **71**, 014015 (2005).
- [52] V. L. Chernyak and I. R. Zhitnitsky, *Nucl. Phys.* **B345**, 137 (1990).
- [53] P. Ball and R. Zwicky, *J. High Energy Phys.* **04** (2006) 046.
- [54] J. Beringer *et al.* (Particle Data Group Collaboration), *Phys. Rev. D* **86**, 010001 (2012).
- [55] M. C. Arnesen, B. Grinstein, I. Z. Rothstein, and I. W. Stewart, *Phys. Rev. Lett.* **95**, 071802 (2005).
- [56] C. G. Boyd, B. Grinstein, and R. F. Lebed, *Phys. Rev. Lett.* **74**, 4603 (1995).
- [57] C. G. Boyd and M. J. Savage, *Phys. Rev. D* **56**, 303 (1997).
- [58] I. Caprini, L. Lellouch, and M. Neubert, *Nucl. Phys.* **B530**, 153 (1998).
- [59] T. Becher and R. J. Hill, *Phys. Lett. B* **633**, 61 (2006).
- [60] C. Bourrely, I. Caprini, and L. Lellouch, *Phys. Rev. D* **79**, 013008 (2009); **82**, 099902(E) (2010).
- [61] A. Bharucha, T. Feldmann, and M. Wick, *J. High Energy Phys.* **09** (2010) 090.
- [62] R. J. Hill, *Proceedings of the Fourth International Conference on Flavor Physics and CP Violation, Vancouver, 2006*, eConf C060409, 027 (2006).
- [63] A. Hocker, H. Lacker, S. Laplace, and F. Le Diberder, *Eur. Phys. J. C* **21**, 225 (2001).
- [64] C. Hambroek, M. Jung, and S. Schacht, LUCY: A Universal Code for Organizing Fits (unpublished).
- [65] S. G. Johnson, <http://ab-initio.mit.edu/nlopt>.
- [66] T. Rowan, Ph.D. thesis, Department of Computer Sciences, University of Texas at Austin, 1990.
- [67] J.-T. Wei *et al.* (BELLE Collaboration), *Phys. Rev. Lett.* **103**, 171801 (2009).
- [68] S. Descotes-Genon, J. Matias, and J. Virto, *Phys. Rev. D* **88**, 074002 (2013).

- [69] W. Altmannshofer and D. M. Straub, *Eur. Phys. J. C* **73**, 2646 (2013).
- [70] F. Beaujean, C. Bobeth, and D. van Dyk, [arXiv:1310.2478](https://arxiv.org/abs/1310.2478).
- [71] R. Aaij *et al.* (LHCb Collaboration), *Phys. Rev. Lett.* **111**, 112003 (2013).
- [72] Z. Ligeti and M. B. Wise, *Phys. Rev. D* **53**, 4937 (1996).
- [73] F. Kruger and L. M. Sehgal, *Phys. Lett. B* **380**, 199 (1996).
- [74] A. Ali, P. Ball, L. T. Handoko, and G. Hiller, *Phys. Rev. D* **61**, 074024 (2000).
- [75] A. V. Manohar and M. B. Wise, *Heavy Quark Physics*, Cambridge Monographs on Particle Physics, Nuclear Physics and Cosmology Vol. 10 (Cambridge University Press, Cambridge, 2007), p. 1. M. A. Shifman, [arXiv:hep-ph/9510377](https://arxiv.org/abs/hep-ph/9510377).